Endocrinology

Adrenomedullin ameliorates pulmonary fibrosis by regulating TGF-β-Smads signaling and myofibroblast differentiation

--Manuscript Draft--

Manuscript Number:	
Full Title:	Adrenomedullin ameliorates pulmonary fibrosis by regulating TGF-β-Smads signaling and myofibroblast differentiation
Article Type:	Research Article
Section/Category:	Growth, Growth Hormone, and Growth Factors
Corresponding Author:	Takayuki Shindo, M.D., Ph.D. Shinshu University Graduate School of Medicine Matsumoto, JAPAN
Other Authors:	Yangxuan Wei
	Megumu Tanaka
	Takayuki Sakurai
	Akiko Kamiyoshi
	Yuka Ichikawa-Shindo
	Hisaka Kawate
	Nanqi Cui
	Shinji Kakihara
	Yunlu Zhao
	Kohsuke Aruga
	Hideki Sanjo
Suggested Reviewers:	Takeshi Tokudome National Cerebral and Cardiovascular Center Research Institute: Kokuritsu Junkankibyo Kenkyu Center Kenkyujo tokudome@ncvc.go.jp A specialist of cardiovascular bioactive molecules including adrenomedullin
	Kazuo Kitamura University of Miyazaki Hospital: Miyazaki Daigaku Igakubu Fuzoku Byoin kazuokit@med.miyazaki-u.ac.jp The scientist who found adrenomedullin
	Tatsuo Shimosawa International University of Health and Welfare tshimo-tky@umin.ac.jp A specialist of cardiovascular bioactive molecules including adrenomedullin
	Toshiro Fujita The University of Tokyo: Tokyo Daigaku Toshiro.FUJITA@rcast.u-tokyo.ac.jp A specialist of cardiovascular bioactive molecules including adrenomedullin
	Naoto Minamino National Cerebral and Cardiovascular Center Research Institute: Kokuritsu Junkankibyo Kenkyu Center Kenkyujo minamino@ncvc.go.jp
Opposed Reviewers:	Kathleen Caron University of North Carolina A competitor generating the similar knockout mouse

	Hiroki Kurihara University of Tokyo A competitor generating the similar knockout mouse
Additional Information:	
Question	**Response**
DATA REPOSITORIES AND DATA REGISTRATION: I have read and agree to take appropriate action to comply with the following Data Repositories and Data Registration guidelines and confirm that I have included the appropriate registration numbers / information in the text of the manuscript being submitted.	Not Applicable
CELL LINE AUTHENTICATION: I have read and understood the Cell Line Authentication policy and describe my submission as follows:	Not applicable to my manuscript.
STEROID HORMONE MEASUREMENT: I have read and understood the Steroid Hormone Measurement policy and describe my submission as follows:	Not applicable to my manuscript.
DATA AVAILABILITY The Endocrine Society requires that authors provide a statement about the availability of data generated or analyzed in the submitted manuscript. Authors are required to include this statement in the final version of accepted manuscripts. For more information, see the Author	Some or all data generated or analyzed during this study are included in this published article or in the data repositories listed in References.

Guidelines. Please select the statement(s) below that describes the availability of the data generated or analyzed in your manuscript. Please include this statement in the manuscript document just before the reference list. Edit the statement to describe and provide means of access, where applicable, by linking to the data or providing the required unique identifier [e.g. the DOI]. This section of the manuscript should be labelled “Data Availability.” If multiple statements are selected, please specify which data applies to each statement.	
SPECIAL REQUESTS: In place of a cover letter, you may enter specific comments or requests to the editors here.	March 30, 2021 Dr. Carol A. Lange Editor-in-Chief, Endocrinology Dear Dr. Lange: We would be very grateful if you would consider our manuscript, entitled “Adrenomedullin ameliorates pulmonary fibrosis by regulating TGF-β-Smads signaling and myofibroblast differentiation” by Yangxuan Wei et al., for publication in Endocrinology. Endogenous bioactive peptides and their receptors play pivotal roles in the maintenance of homeostasis, and they are considered to be important drug targets for the treatment of various diseases. Adrenomedullin (AM) is a peptide hormone originally identified as a vasodilator. Using gene engineering to alter expression of AM and its related molecules in mice, we have reported on the various pathophysiological functions of AM in vivo. We and other groups have shown that AM’s functions are regulated by receptor activity-modifying protein 2, or RAMP2: homozygous AM or RAMP2 knockout is embryonically lethal. In the present study, we investigated the pathophysiological significance of the AM-RAMP2 system in the lung using the bleomycin (BLM)-induced pulmonary fibrosis model in mice. In heterozygous AM (AM+/-) or RAMP2+/- knockout mice, inflammation during the early acute phase and fibrosis during the later chronic phase were both exacerbated compared to control wild-type mice. Contrary, AM administration suppressed the severity of fibrosis. The TGF-β-Smads pathway is a major mediator of tissue fibrosis. In the lungs of BLM-administered AM+/- mice, activation of Smad3, a receptor activated Smad, was enhanced, whereas Smad7, an antagonistic Smad, was downregulated. We also found that miR-21, a pro-fibrotic microRNA that targets and suppresses Smad7, was upregulated. TGF-β-stimulated lung fibroblasts derived from AM+/- mice, preferentially differentiated into myofibroblasts. Notably, nonproliferating myofibroblasts (non-p-MyoFbs), which are larger in size and show greater contractility with higher α-SMA expression and greater production of extracellular matrix and chemokines, but lower proliferative capacity, were specifically increased in AM+/- mice. We suggest that non-p-MyoFbs are related to the severity of pulmonary fibrosis.

	These observations indicate that in addition to suppressing inflammation during the early phase of fibrosis, the AM-RAMP2 system also suppresses fibrosis progression by regulating miR-21 expression, the TGF-β-Smads pathway, and non-p-MyoFb differentiation during the chronic phase. This makes the AM-RAMP2 system a promising new target for the treatment of pulmonary fibrosis, for which there are currently limited therapeutic options. We believe this paper will be of great interest to the readers of Endocrinology. The manuscript has not been published and is not being considered for publication elsewhere in whole or in part in any language. Dr. Kathleen Caron (University of North Carolina) and Hiroki Kurihara (University of Tokyo) are our competitors generating the same gene-engineered mice, so please do not send them our manuscript. We would like to suggest potential reviewers: Dr. Takeshi Tokudome Department of Biochemistry, National Cerebral and Cardiovascular Research Center Email; tokudome@ncvc.go.jp Dr. Kazuo Kitamura Division of Circulatory and Body Fluid Regulation, Faculty of Medicine, University of Miyazaki Email; kazuokit@med.miyazaki-u.ac.jp Dr. Tatsuo Shimosawa Department of Clinical Laboratory, School of Medicine, International University of Health and Welfare Email; tshimo-tky@umin.ac.jp Dr. Toshiro Fujita Division of Clinical Epigenetics, Research Center for Advanced Science and Technology, the University of Tokyo Email; Toshiro.FUJITA@rcast.u-tokyo.ac.jp Dr. Naoto Minamino Omics Research Center, National Cerebral and Cardiovascular Research Center Email; minamino@ncvc.go.jp Yours sincerely, Takayuki Shindo, MD, PhD, Department of Cardiovascular Research, Shinshu University School of Medicine 3-1-1 Asahi, Matsumoto 390-8621, Japan E-mail: tshindo@shinshu-u.ac.jp Tel: +81-263-37-2578 Fax: +81-263-37-3437
Funding Information:	Japan Agency for Medical Research and

	Development	Dr. Takayuki Shindo
	Core Research for Evolutional Science and Technology	Dr. Takayuki Shindo
	SENSHIN Medical Research Foundation	Dr. Takayuki Shindo
	NOVARTIS Foundation (Japan) for the Promotion of Science	Dr. Takayuki Shindo
	Akaeda Medical Research Foundation	Dr. Takayuki Shindo
	Takahashi Industrial and Economic Research Foundation	Dr. Takayuki Shindo
	Naito Foundation	Megumu Tanaka
	Uehara Memorial Foundation	Megumu Tanaka
	Takeda Science Foundation	Megumu Tanaka
	Mochida Memorial Foundation for Medical and Pharmaceutical Research	Megumu Tanaka
	Nakatomi Foundation	Megumu Tanaka
	Yamaguchi Endocrine Research Foundation	Akiko Kamiyoshi
	Japan Student Services Organization (JP)	Yangxuan Wei
Requested Editor:		
Author Comments:	Disclosures: Sources of funding This study was supported by Grants-in-Aid for Scientific Research (KAKENHI), Core Research for Evolutionary Science and Technology (CREST) of Japan Science and Technology Agency (JST) and the Japan Agency for Medical Research and Development (AMED), a SENSHIN Medical Research Foundation grant, a NOVARTIS Foundation (Japan) for the Promotion of Science grant, an Akaeda Medical Research Foundation grant, a Hoyu Science Foundation grant, a Takahashi Industrial and Economic Research Foundation grant , a Bristol-Myers Squibb research grand and a The Japan Research Institute of Industrial Science grant to T.S. A Naito Foundation grant, a Japan Heart Foundation Dr. Hiorshi Irisawa & Dr. Aya Irisawa Memorial Research Grant, a Kanzawa Medical Research Foundation grant, The Uehara Memorial Foundation grant, a Fund of Nagano Prefecture to promote scientific activity, Takeda Science Foundation grant, a Mochida Memorial Foundation for Medical and Pharmaceutical Research grant, and The Nakatomi Foundation grant to MT. A NOVARTIS Foundation (Japan) for the Promotion of Science grant to TS. A Yamaguchi Endocrine Research Foundation grant to AK. Y.W received a scholarship from Japan Student Services Organization. Authors' contributions YW carried out the experiments and wrote the manuscript. MT helped gene expression analysis. TS and AK generated genetically engineered mice. YI and HK helped histological analysis. NC and SK helped Western blot analysis. YZ and KA helped cellular experiments. HS helped FACS analysis. TS planned the experiments and supervised the manuscript. Conflicts of interest The authors declare no conflicts of interest associated with this manuscript.

Adrenomedullin ameliorates pulmonary fibrosis by regulating TGF-β-Smads signaling and myofibroblast differentiation

Yangxuan Wei[1], Megumu Tanaka[1], Takayuki Sakurai[1, 2], Akiko Kamiyoshi[1, 2], Yuka Ichikawa-Shindo[1], Hisaka Kawate[1], Nanqi Cui[1], Shinji Kakihara[1], Yunlu Zhao[1], Kohsuke Aruga[1], Hideki Sanjo[3], Takayuki Shindo[1, 2]

[1]Department of Cardiovascular Research, Shinshu University School of Medicine, Japan
[2]Department of Life Innovation, Institute for Biomedical Sciences, Interdisciplinary Cluster for Cutting Edge Research, Shinshu University, Japan
[3]Department of Molecular and Cellular Immunology, Shinshu University School of Medicine, Japan

Short running head: Amelioration of pulmonary fibrosis by AM

Number of text pages 42
Number of tables 1
Number of figures 16
Number of supplementary figures 9

Address for correspondence
Takayuki Shindo, MD, PhD
Department of Cardiovascular Research,
Shinshu University School of Medicine
Asahi 3-1-1, Matsumoto, Nagano, 390-8621, Japan
Tel: +81-263-37-2578
Fax: +81-263-37-3437
Email: tshindo@shinshu-u.ac.jp

Disclosures:

Sources of funding

This study was supported by Grants-in-Aid for Scientific Research (KAKENHI), Core Research for Evolutionary Science and Technology (CREST) of Japan Science and Technology Agency (JST) and the Japan Agency for Medical Research and Development (AMED), a SENSHIN Medical Research Foundation grant, a NOVARTIS Foundation (Japan) for the Promotion of Science grant, an Akaeda Medical Research Foundation grant, a Hoyu Science Foundation grant, a Takahashi Industrial and Economic Research Foundation grant, a Bristol-Myers Squibb research grand and a The Japan Research Institute of Industrial Science grant to T.S.

A Naito Foundation grant, a Japan Heart Foundation Dr. Hiorshi Irisawa & Dr. Aya Irisawa Memorial Research Grant, a Kanzawa Medical Research Foundation grant, The Uehara Memorial Foundation grant, a Fund of Nagano Prefecture to promote scientific activity, Takeda Science Foundation grant, a Mochida Memorial Foundation for Medical and Pharmaceutical Research grant, and The Nakatomi Foundation grant to MT.

A NOVARTIS Foundation (Japan) for the Promotion of Science grant to TS.

A Yamaguchi Endocrine Research Foundation grant to AK.

Y.W received a scholarship from Japan Student Services Organization.

Authors' contributions

YW carried out the experiments and wrote the manuscript. MT helped gene expression analysis. TS and AK generated genetically engineered mice. YI and HK helped histological analysis. NC and SK helped Western blot analysis. YZ and KA helped cellular experiments. HS helped FACS analysis. TS planned the experiments and supervised the manuscript.

Conflicts of interest

The authors declare no conflicts of interest associated with this manuscript.

Abstract

Pulmonary fibrosis is an irreversible, potentially fatal disease. Adrenomedullin (AM) is a multifunctional peptide whose activity is regulated by receptor activity-modifying protein 2 (RAMP2). In the present study, we used the bleomycin (BLM)-induced mouse pulmonary fibrosis model to investigate the pathophysiological significance of AM-RAMP2 system in the lung. In heterozygous AM knockout mice (AM+/-), hydroxyproline content and Ashcroft score representing the fibrosis severity were significantly higher than in wild-type mice (WT). During the acute phase after BLM administration, FACS analysis showed significant increases in eosinophil, monocyte, and neutrophil infiltration into the lungs of AM+/-. During the chronic phase, fibrosis-related molecules were upregulated in AM+/-. These changes were also confirmed in RAMP2+/-. Contrary, AM administration suppressed the severity of fibrosis. In the lungs of BLM-administered AM+/-, the activation level of Smad3, a receptor-activated Smad, was higher than in WT. Smad7, an antagonistic Smad, was downregulated, and microRNA 21, which targets Smad7, was upregulated compared to WT. Isolated AM+/- lung fibroblasts showed lower proliferation and migration capacity than WT fibroblasts. Stimulation with TGF-β increased the number of α-SMA-positive myofibroblasts, which were more prominent among AM+/- cells. TGF-β-stimulated AM+/- myofibroblasts were larger and exhibited greater contractility and extracellular matrix production than WT cells. These cells were α-SMA (+), F-actin (+) and Ki-67(-) and appeared to be nonproliferating myofibroblasts (non-p-MyoFbs), which contribute to the severity of fibrosis. From these results, we suggest that in addition to suppressing inflammation, the AM-RAMP2 system ameliorates pulmonary fibrosis by suppressing TGF-β-Smad3 signaling, microRNA-21 activity and differentiation into non-p-MyoFbs.

Non-standard Abbreviations

AM: Adrenomedullin

RAMP: Receptor activity-modifying protein

CLR: Calcitonin receptor-like receptor

BLM: Bleomycin

WT; wild-type

α-SMA; α-smooth muscle actin

MT; Masson trichrome

TGF-β; transforming growth factor-β

non-p-MyoFb: nonproliferating myofibroblasts

Key Words

Adrenomedullin ■ RAMP2 ■ Pulmonary fibrosis ■ Myofibroblast ■ TGF-β ■ Smad ■ microRNA-21

Introduction

Idiopathic interstitial pneumonia is an intractable disease in which pulmonary fibrosis gradually progresses over a chronic course in most cases. As respiratory failure worsens, the patient's quality of life is significantly reduced, and the average survival time after diagnosis is reportedly only 3 to 5 years (1,2). Although several antifibrotic drugs have been launched in recent years, they provide little relief to this group of patients. Consequently, providing patients suffering from idiopathic interstitial pneumonia and pulmonary fibrosis with therapeutic drugs with new mechanisms of action is expected to improve their quality of life and prognosis.

Adrenomedullin (AM) is a 52-amino acid vasodilating peptide first identified from human pheochromocytoma (3). AM is now known to play important roles in circulatory regulation and the pathogenesis of cardiovascular disease, and is, itself, is a promising therapeutic agent for the treatment of cardiovascular disease. Although AM is mainly secreted in the cardiovascular system, it is widely distributed in numerous tissues and organs (4), where it functions as a local autocrine/paracrine mediator exhibiting anti-inflammatory, anti-oxidative, anti-apoptotic and antifibrotic effects, among others (5). AM production and secretion are induced by inflammatory cytokines such as tumor necrosis factor-α and interleukin (IL)-1. Conversely, AM induces downregulation of inflammatory cytokines in cultured cells and various animal models (6). In fact, AM is currently undergoing clinical trials for patients with chronic and refractory inflammatory bowel disease (7,8).

We have generated various mouse knockout models for AM and related molecules. Using those models, we previously observed that homozygous AM knockout (AM-/-) is embryonically lethal at midgestation, with systemic edema and bleeding that are mainly caused by abnormal vascular development (9). These observations make it clear that AM is essential for proper development of the vascular system. On the other hand, heterozygous AM knockout mice (AM+/-) survive, though their AM levels are reduced by about half. Interestingly, AM+/- mice are prone to the development of inflammation and fibrosis (10-12). Conversely, transgenic mice overexpressing AM exhibit resistance to various forms of organ damage (9,13,14), suggesting AM acts as an anti-inflammatory, anti-fibrotic and organ-protective factor.

AM is a member of the calcitonin superfamily and acts via a G protein-coupled 7-

transmembrane domain receptor, calcitonin receptor-like receptor (CLR) (15). The specificity of CLR for its ligands is regulated by three receptor activity-modifying proteins, RAMP1, -2 and -3 (16). Interestingly, among RAMP knockout mice, only homozygous RAMP2 knockout mice (RAMP2-/-) die at midgestation and reproduce the phenotypes observed in AM-/- mice (17). RAMP2 thus appears to be the key determinant of AM's function during vascular development. As conventional RAMP2 knockout is lethal, we generated vascular endothelial cell-specific RAMP2-/- mice. In these mice, we observed marked accumulation of inflammatory cells around blood vessels and, with aging, spontaneous development of organ fibrosis (18). These results suggest the AM-RAMP2 system is deeply involved in the pathogenesis of inflammation and fibrosis, which in turn raises the possibility of new treatments targeting the activity of the AM-RAMP2 system.

Bleomycin (BLM) is a chemotherapeutic agent used to treat cancer, but one of its side effects is pulmonary toxicity. In a BLM-induced pulmonary fibrosis model, it is thought that intratracheally administered BLM directly damages alveolar epithelial cells, leading to the infiltration of inflammatory cells and the development of interstitial fibrosis (19). In the present study, we used the BLM-induced pulmonary fibrosis model to evaluate the pathophysiological significance of AM-RAMP2 and to establish a basis for the treatment and prevention of pulmonary fibrosis using AM itself or through regulation of the AM-RAMP2 system.

Methods

Animals

Because homozygous AM or RAMP2 knockout is lethal in utero, we used heterozygous AM (AM+/-) and RAMP (RAMP2+/-) knockout mice, which were previously generated in our group (9,17). In these mice, expression of the affected genes is reduced to approximately half that in wild-type (WT) mice. WT littermates from each knockout mouse line were used as controls. The background of mice used in this study was C57BL/6J. For time course observation of the BLM-induced pulmonary fibrosis model and experiments entailing exogenous administration of AM, male C57BL/6J mice purchased from Charles River Laboratories Japan (Kanagawa, Japan) were used. All mice were maintained according to a strict procedure under specific pathogen-free conditions in an environmentally controlled (12 h light/dark cycle; room temperature, 22 ± 2 °C) breeding room at the Division of Laboratory Animal Research, Department of Life Science, Research Center for Human and Environmental Sciences, Shinshu University. All animal experiments were conducted in accordance with the ethical guidelines of Shinshu University, the Declaration of Helsinki and the NIH Guide for the Care and Use of Laboratory Animals. All experiments were approved by the Shinshu University Ethics Committee for Animal Experiments. Before all invasive procedures, mice were anesthetized through intraperitoneal injection with a combination of 0.3 mg/kg medetomidine (Nippon Zenyaku Kogyo Co. Ltd., Koriyama Japan), 4.0 mg/kg midazolam (Astellas Pharma Inc. Tokyo Japan) and 5.0 mg/kg butorphanol (Meiji Seika Pharma Co. Ltd., Tokyo Japan).

BLM-induced pulmonary fibrosis model

Ten- to 12-week-old male AM+/-, RAMP2+/- and WT mice weighing 25 g were intratracheally instilled with 2 mg/kg BLM (NIPPON KAYAKU, Tokyo, Japan) in 50 μl of sterile saline. The lungs were subsequently removed 3 to 28 days after BLM administration. Left lungs were formalin fixed, paraffin embedded and used for histological analysis. Right lungs were snap frozen and processed for mRNA. Left lungs were also used for hydroxyproline content measurements.

196 **Administration of AM to mice**

197 Ten- to 12-week-old male C57BL/6J mice weighing 25 g (Charles River
198 Laboratories Japan) were administered recombinant human AM (provided by Dr. Kenji
199 Kangawa) as described previously (20). Using an osmotic pump (Alzet; DURECT Co,
200 Cupertino, CA), mice in the AM-treated group received continuous subcutaneous
201 administration of AM dissolved in sterile saline. The saline-treated group was used as a
202 control. The infusion rate was 0.05 μg/kg/min. Infusion was started 1 day before BLM-
203 administration and was continued for an additional 3, 7 or 14 days. The effectiveness of
204 human AM in mice is well established (21,22), and the dosage used was selected based
205 on earlier studies (23,24).
206

207 **Hydroxyproline assay**

208 Hydroxyproline assays (Quick Zyme Biosciences, Leiden, The Netherlands) were
209 performed as described previously (25). Briefly, left lungs were homogenized in 6 N
210 hydrochloric acid and hydrolyzed for 20 h at 95°C. After hydrolysis, the tubes were
211 cooled to room temperature and then centrifuged for 10 min at 13,000 rpm, after which
212 the hydrolyzed samples were diluted with water to 4 M HCl, and 35-μl aliquots of
213 standard solution and 4 M HCl samples were pipetted into the appropriate wells. Assay
214 buffer was then added and incubated for 20 min at room temperature while shaking the
215 plate. A mixture of reagents A and B (2:3) was then added, and the samples were
216 incubated at 60°C for 60 min. After cooling the samples to room temperature, absorbance
217 was measured at 570 nm. The hydroxyproline content was determined against a standard
218 curve generated with pure hydroxyproline.
219

220 **FACS analysis**

221 Total lungs were minced into 1 mm pieces and digested for 30 min at 37°C with
222 gentle shaking in 20 ml of Hanks' balanced salt solution (HBSS (+); Wako, Osaka, Japan)
223 supplemented with 0.5 mg/ml collagenase IV (Sigma-Aldrich, St. Louis, MO) and 50
224 U/ml DNase I (Wako). Single-cell suspensions were then filtered through a cell strainer
225 (mesh 100 μm) (AS ONE, Osaka, Japan), and cells resuspended in 1 ml of HBSS with
226 2% FBS were counted using a microscopic counting chamber. After excluding the dead
227 cells using trypan blue, the cell density was adjusted to 1-10 x 10^6 cells/ml. The cells were

then centrifuged to remove the supernatant, after which the Fc Block reaction was run for 10 min at 4℃ followed by staining with fluorochrome-conjugated antigen-specific antibodies for 20 min at 4℃ in the dark. After suspending the cells in 700 µl of FACS buffer (1x PBS, 1% BSA, 2 nM EDTA, 0.05% NaN3) in a glass tube, 10 µl of 20 µg/ml propidium iodide (PI) was added to each tube.

The regents and fluorochrome-conjugated antibodies used in this research were as follows: TCRβ (H57-597) (RRID: AB_2562562, Cat# 109230) (26), MHC II (M5/114.15.2) (RRID: AB_2290801, Cat# 107629) (27), CD11b (M1/70) (RRID: AB_2629529, Cat# 101263) (28), CD11c (HL3) (RRID: AB_2562414, Cat# 117339) (29), Ly6c (HK1.4) (RRID: AB_2565852, Cat# 128041) (30), Ly6G (1A8) (RRID: AB_1236488, Cat# 127605) (31), CD4 (RM4-5) (RRID: AB_2563054, Cat# 100548) (32), all from BioLegend (San Diego, CA); SiglecF (E50-2440) (RRID: AB_10896143, Cat# 562068) (33), NK1.1 (PK136) (RRID: AB_10563422, Cat# 561117) (34) from BD Bioscience (San Jose, CA); CD45 (30-F11) (RRID: AB_1548790, Cat# 47-0451-80) (35) from Thermo Fisher Scientific (Carlsbad, CA). Anti-CD16/CD32 (Mouse Fc Block) (2.4G2) (RRID: AB_394657, Cat# 553142) (36) from BD Bioscience. PI was purchased from Sigma-Aldrich. Stained cells were analyzed using a FACS Celesta flow cytometer (BD Bioscience). Flow cytometry data were analyzed with Kaluza software (Beckman Coulter, Brea, CA). Gating was performed as shown in Supplementary Figure 1.

Real-time qPCR analysis

Total RNA was prepared using TRI REAGEN (Molecular Research Center, Cincinnati, OH) and a DNA-free DNA Removal kit (Ambion, Naugatuck, CT) according to the manufacturer's instructions. For cDNA synthesis, RNA was reverse-transcribed using a High Capacity cDNA Reverse Transcription Kit (Applied Biosystems, Foster City, CA). PCR primers and probes were designed using NCBI Primer-BLAST (https://www.ncbi.nlm.nih.gov/tools/primer-blast/) and synthesized by Integrated DNA Technologies (Coralville, IA). The primers and probes used are listed in Table 1. qRT-PCR was performed using SYBR Green (Toyobo, Osaka, Japan) or Realtime PCR Master Mix (Toyobo) and TaqMan probes (MBL, Aichi, Japan) on an ABI Prism 7300 Sequence Detection System (Applied Biosystems). The cycling conditions were 50°C for 2 min and 95°C for 2 min, followed by 40 cycles of 95°C for 15 s and 60°C for 1 min.

Relative mRNA levels were normalized to mouse glyceraldehyde-3-phosphate dehydrogenase mRNA (Pre-Developed TaqMan assay reagents; Applied Biosystems) and calculated using the comparative cycle threshold method (ΔΔCt).

Real-time qPCR analysis of microRNA-21 expression

A miRNeasy Mini Kit (QIAGEN, Venlo, Nederland) was used to purify the cellular microRNA. The specific primers were as follows: for microRNA-21 (miR-21), 5'-UAGCUUAUCAGACUGAUGUUGA-3' (mmu-miR-21a-5p, MIMAT0000530, QIAGEN) and for normalization control RNA U6, 5'-GUGCUCGCUUCGGCAGCACAUAUACUAAAAUUGGAACGAUACAGAGAAG AUUAGCAUGGCCCCUGCGCAAGGAUGACACGCAAAUUCGUGAAGCGUUCC AUAUUUUU-3' (Hs_RNU6-2_11 MS00033740, QIAGEN). For cDNA synthesis, RNA was reverse-transcribed using a miScript Reverse Transcription Kit (QIAGEN), and a miScript SYBR Green PCR Kit was used according to the manufacture's instructions (QIAGEN). Quantitative real-time RT-PCR was performed using a StepOnePlus real-time PCR system (Thermo Fisher Scientific).

Histological examination

Lung sections were fixed in 4% formalin neutral buffer, embedded in paraffin, and cut into 4-μm-thick sections. Some sections were used for hematoxylin/eosin (H&E) and Masson trichrome staining. Immunohistochemical staining was performed using anti-CD45 (RRID: AB_357485，Cat# MAB114, Wako, Osaka, Japan) (37), anti-F4/80 (RRID: AB_323806, Cat# MCA497GA, BioRad, Hercules, CA) (38), anti-CD3 (RRID: AB_305055, Cat# ab5690, Abcam, Cambridge, England) (39), and anti-α-SMA (RRID: AB_2223500, Cat# M0851, Dako) (40) antibodies. Biotin-conjugated secondary antibodies and 3,3′-diaminobenzidine (DAB) (Histofine kit, Nichirei, Tokyo, Japan) were used to visualize the labeling of α-SMA, CD3 or F4/80. A VECTASTAIN ABC kit (Vector Laboratories, Burlingame, CA) was used to visualize CD45 labeling, and the nuclei were counterstained with hematoxylin. Inspections were performed using a microscope (BZ-X710; Keyence, Osaka, Japan). Quantification was performed using a BZ analyzer (Keyence).

Modified Ashcroft score

Pulmonary fibrosis severity was scored using a modified Ashcroft score (41). Based on the histological features of the pulmonary fibrosis, the severity was graded from 0 (Alveolar septa: no fibrotic burden at the most flimsy small fibers in some alveolar walls. Lung structure: Normal lung) to 8 (Alveolar septa: nonexistent. Lung structure: microscope fields show complete obliteration with fibrotic masses).

Western blot analysis

Lungs and cells were lysed in an ice-cold RIPA Lysis Buffer System (Santa Cruz Biotechnology, Santa Cruz, CA) supplemented with PosSTOP phosphatase inhibitor (Roche Applied Science, Upper Bavaria, Germany) and then sonicated. Samples of the resultant lysate (1 μg/well for cells, 10 μg/well for the lungs) were subjected to electrophoresis in TGX gel (Bio-Rad Laboratories, Hercules, CA), and the resolved proteins were transferred to PVDF membranes (Bio-Rad Laboratories). After blocking with 5% skim milk, the membranes were incubated and probed using primary antibodies against Smad2 (RRID: AB_10626777，Cat# 5339S) (42), Smad3 (RRID: AB_2193182，Cat# 9523S) (43), p-Smad3 (RRID: AB_2193207，Cat# 9520S) (44) (Cell Signaling Technology, Danvers, MA) at 1:1000 dilution, p-Smad2 (RRID: AB_2889838, Cat# ab184557) (45) and Smad7 (RRID: AB_2889839, Cat# ab216428) (46) (Abcam) at 1:1000 dilution, followed by appropriate secondary antibodies (Santa Cruz). Anti-β-actin antibody (RRID: AB_2223172 ，Cat# 4970S, Cell Signaling Technology) (47) at 1:8000 dilution served as a loading control. The bound antibodies were visualized using chemiluminescent horseradish peroxidase substrate (Merck Millipore, Burlington, MA), and the chemiluminescence was analyzed using an Image Quant LAS 4000 system (GE Healthcare). Levels of Smad2 and Smad3 activation were determined based on the ratio of band intensities after blotting with antibodies specific for the phosphorylated and unphosphorylated proteins. For quantification, images of the blots were captured and analyzed using Image Quant TL software (GE Healthcare).

Isolation of lung fibroblasts

Mouse lung fibroblasts were established as described previously (48). Fresh samples collected from lungs were washed with serum-free Dulbecco's modified Eagle medium (DMEM; Wako), finely minced into small pieces of approximately 0.5-1.0 mm and digested enzymatically with 2 mg/ml collagenase type I (Wako) in DMEM for 3 h at 37 °C. After cell dissociation, the samples were filtered through a cell strainer (mesh 40 μm) (AS ONE, Osaka, Japan), centrifuged, washed with PBS and cultured in 3.5 cm dishes in DMEM supplemented with 10% FBS and 1% penicillin-streptomycin. Cells were allowed to grow on the plate for 4 days. During that period, the medium was replenished every 2 days. To ensure minimal contamination of epithelial cells prior to their use in experiments, the cells were tested to confirm >95% positive staining for vimentin and negative staining for E-cadherin. Primary cultured pulmonary fibroblasts with 3-4 passages were used for experiments.

TGF-β-stimulation of primary cultured lung fibroblasts

Cultured lung fibroblasts were pre-treated with AM (10^{-7} M) or PBS for 2 h followed by treatment with transforming growth factor-β1 (TGF-β1) (10 ng/mL) for 24 h. The dosage and treatment period were chosen based on previous studies (49-51). In some experiments, the cells were also treated for 24 h with 10 μM SB431542 (Cayman Chemical, Ann Arbor, MI), a selective TGF-β receptor 1 (TGFβR1) inhibitor (52). Alternatively, cells were pre-treated with 3 μM SIS3 (Merck, Darmstadt, Germany), a selective Smad3 inhibitor (53), for 1 h followed by treatment with TGF-β1 (10 ng/mL) for 24 h (53).

For immunostaining, plates were dipped in 4% paraformaldehyde for 10 min, blocked, and immunostained with anti-α-SMA (Code# M0851, Dako) (40), anti-vimentin (RRID: AB_10562134, Cat# ab92547, Abcam) (54) or anti-Ki67 (RRID: AB_443209, Cat# ab15580, Abcam) (55) antibodies. Cells were also stained with phalloidin (Thermo Fisher Scientific) to visualize actin fibers. Nuclei were counterstained using DAPI (Thermo Fisher Scientific). Cells were then examined under a fluorescence microscope (BZ-X710). Positive areas were determined using Hybrid Cell Count (BZ analyzer) under the same conditions.

Gel contraction assay

Collagen gel contraction assays were performed according to the manufacturer's instructions (Cell Biolabs; San Diego, CA) (56). Briefly, cells were pre-treated for 2 h with AM (10^{-7} M) or PBS followed by stimulation for 24 h with TGF-β1 (10 ng/mL). The cells were then collected from plates and suspended at a density of 4.0×10^5 cells per 100 µl of medium to which 400 µl of neutralized collagen solution were added. The resultant mixture was added to one well of a 24-well culture plate and allowed to gel for 2 h at 37 °C. After polymerization, 1.0 mL of culture medium was added on top of the gel lattice and incubated for 24 h. The stress was released by running a sterile pipette tip along the sides of the well. The culture dish was then scanned 12 h after the stress was released. The area of the collagen gel was measured using ImageJ software version 1.53f (NIH, Bethesda, MD; http://imagej.nih.gov/ij).

Cell proliferation assay

One hundred-microliter aliquots of fibroblasts suspended at a density of 5×10^4 cells/ml in DMEM containing 10% FBS were plated in 96-well plates and incubated for 24 h. The cells were then treated with 10 ng/ml TGF-β1 for 24 h, after which the culture medium was changed and 10 µl of Cell Counting Kit-8 (CCK-8) solution (Dojindo, Kumamoto, Japan) were added to each well. The plate was then incubated for 1 h at 37°C in the incubator, and the absorbance at 450 nm was measured using a microplate reader. Experiments were performed 4 times independently.

Scratch assay

For scratch assays, cells were plated in 6-well plates at 2×10^5 cells/well, treated with TGF-β1 (10 ng/ml) and grown into a monolayer. The assays were performed as described previously (57). Briefly, 5 µg/ml mitomycin C (Kyowa Kirin, Tokyo, Japan) was added to the medium for 3 h to block cell proliferation, and a linear scratch/wound was made on the cell monolayer using a sterile pipette. Photomicrographs were taken of the culture at 40x magnification, and the distance migrated was observed within appropriate times. The distances were measured using CellSens standard software (OLYMPUS, Tokyo, Japan). Experiments were performed 3 times independently.

385 **Downregulation of miR-21**

386 Downregulation of miR-21 was performed as described previously (58). The miR-
387 21 inhibitor, LNA-5'-UCAACAUCAGUCUGAUAAGCUA-3', a chemically modified
388 and optimized oligonucleotide designed to specifically target the microRNA molecule
389 in cells, and its negative control, LNA-5'-CAGUACUUUUGUGUAGUACAA-3', were
390 purchased from Genepharma (Shanghai, China). Cells were transfected with the
391 oligonucleotides using Lipofectamine 3000 (Thermo Fisher Scientific) at a final
392 concentration of 100 nM following the manufacturer's instructions. The efficiency of
393 transfection was assessed with miR-21 qPCR (StepOnePlus real-time PCR system,
394 Thermo Fisher Scientific) and fluorescence microscopy (BZ-X710).
395
396 **Statistics**

397 Statistical analysis was performed with GraphPad Prism software version 7.03.
398 (GraphPad Software Inc., San Diego, CA). Quantitative values are expressed as the mean
399 ± SEM. The significance of differences was assessed using Student's t test, one-way
400 ANOVA with Tukey's or Dunnett's test, or two-way ANOVA with Tukey's test. Values
401 of $p<0.05$ were considered significant. "*" represents compared between the groups, "#"
402 represents compared with control WT mice, "†" represents compared with control
403 knockout mice. *, #, † represent $p<0.05$, **, ##, †† represent $p<0.01$ and ***, ###, †††
404 represent $p<0.001$.
405

406 **Results**

407 **Time course of the pathogenesis of bleomycin-induced pulmonary fibrosis**

408 C57BL/6J WT mice were intratracheally administered bleomycin (BLM) to induce
409 pulmonary fibrosis. Lung weights and lung weight / body weight ratios were increased
410 from day 3 to day 14 after BLM administration (Supplementary Figure 2A-C). The
411 expression of genes encoding AM's receptor, CLR, and RAMP2 and RAMP3 (*Calcrl,*
412 *Ramp2* and *Ramp3*) gradually declined over the 28-day observation period after BLM
413 administration (Supplementary Figure 2D). Expression of the gene encoding AM (*Adm*)
414 was transiently and significantly elevated on day 3 after BLM administration but returned
415 to the control level by day 7, and then continued to decline until day 28. This indicates
416 that *Adm* expression was strongly induced during the acute phase of the response to BLM
417 and there was a compensatory downregulation of AM's receptor system, which suggests
418 AM has important pathological significance in the BLM-induced lung injury.

419 BLM-induced pulmonary fibrosis progresses from inflammation to collagen
420 deposition leading to interstitial fibrosis (59). Expression of genes encoding
421 inflammation-related factors, such as IL-6 and MCP-1 (*Il-6, Ccl2*), peaked on day 3 after
422 BLM administration then gradually decreased until day 28, suggesting that marked
423 inflammation was induced during the acute phase and then gradually disappeared
424 (Supplementary Figure 2E, F). Expression of the gene encoding α-SMA (*Acta2*), a
425 myofibroblast marker, as well as the fibrosis-related factors fibronectin and type I
426 collagen α1 (*Fn1, Col1a1*) peaked on day 14 after BLM administration but had decreased
427 by day 28. In addition, expression of the gene encoding osteopontin (*Spp1*), which is
428 related to both inflammation and fibrosis, was elevated on days 7 and 14 and had
429 decreased slightly, but remained elevated, on day 28 (Supplementary Figure 2G-J). These
430 results indicate that a strong fibrotic response occurred during the later phase, beginning
431 14 days after BLM administration.

432 The pathological changes in the lungs after BLM administration were then
433 observed (Supplementary Figure 3A). Modified Ashcroft scores, which indicate the
434 severity of pulmonary fibrosis, and the fibrotic area peaked on day 14 after BLM
435 administration (Supplementary Figure 3B, C). The area positive for α-SMA-
436 immunostaining was largest at 14 days, which was temporally consistent with the change
437 in its gene expression (Supplementary Figure 3D). By contrast, the numbers of CD45-

positive leukocytes (Supplementary Figure 3E), CD3-positive T cells (Supplementary Figure 3F) and F4/80-positive macrophages (Supplementary Figure 3G) peaked on day 7. These pathological findings are consistent with the results of gene expression indicating a strong inflammatory response during the acute phase after BLM administration (day 3 to 7) and a strong fibrotic response during the later phase (day 14 to 28).

Pulmonary fibrosis is exacerbated in both AM+/- and RAMP2+/- mice

To determine the pathophysiological significance of endogenous AM in pulmonary fibrosis, we compared BLM-induced pulmonary fibrosis between AM knockout (AM+/-) mice and their wild-type (WT) littermates. Although there was no significant difference in survival after BLM administration, AM+/- mice tended to have a lower survival rate than WT mice over time (Supplementary Figure 4). Lung weight increased over time in both groups but was significantly greater in AM+/- than WT mice on days 14 and 28 (Figure 1A-C). To quantify the amount of collagen in the tissues, hydroxyproline levels were measured in the lung and were found to be was significantly higher in AM+/- than in WT mice on day 14 (Figure 1D).

Gene expression analysis showed that *Il-6* expression was significantly higher in AM+/- than WT mice during the earlier phase after BLM administration (day 3) (Figure 1E), and *Ccl2* expression also tended to be upregulated (Figure 1F). By contrast, *Acta2* expression was significantly higher in AM+/- than WT mice on day 14 (Figure 1J), *Spp1* on day 28, and *Col1a1* and *Fn1* on days 14 and 28 (Figure 1G-I) after BLM administration. Pathological analysis showed that AM+/- lungs exhibited significantly increased inflammatory cell infiltration during the acute phase (Figure 2B, F-H) and significantly increased fibrosis and α-SMA expression during the chronic phase (Figure 2A, C-E).

Because the pathological findings showed increased infiltration of inflammatory cells during the acute phase in AM+/- lungs, we performed a FACS analysis to quantitatively evaluate each leukocyte fraction (Figure 3A-C). When the inflammatory cell infiltration was followed chronologically, the numbers of eosinophils, monocytes and neutrophils were significantly higher in AM+/- than WT mice during the acute phase after BLM administration (Figure 3D). These findings indicate that endogenous AM suppresses inflammation during the acute phase and fibrosis during the chronic phase

after BLM administration.

Among RAMPs, RAMP2 is highly expressed in the lung. We previously showed that the anti-inflammatory and antifibrotic effects of AM are mainly regulated by RAMP2 and that endothelial cell-specific RAMP2 knockout leads to strong inflammatory cell infiltration around blood vessels and progression of organ fibrosis with aging (60). To clarify whether the suppressive effect of endogenous AM on pulmonary fibrosis is mediated by RAMP2, BLM-induced fibrosis was compared between RAMP2 knockout (RAMP2+/-) mice and their WT littermates. The results were nearly identical to those obtained with AM+/- mice. That is, RAMP2+/- mice had heavier lung weights (Supplementary Figure 5A-C) and higher hydroxyproline contents (Supplementary Figure 5D) than WT mice. In addition, gene expression of inflammatory cytokines was upregulated during the acute phase (Supplementary Figure 5E, F), and gene expression of fibrosis-related genes was upregulated during the chronic phase (Supplementary Figure 5G-J). Pathological findings were also similar to those of AM+/- mice, with greater inflammatory cell infiltration during the acute phase (Supplementary Figure 6B, F-H) and greater fibrosis during the chronic phase in RAMP2+/- than WT mice (Supplementary Figure 6A, C-E). These results suggest that the inhibitory effects of endogenous AM on inflammation and fibrosis are mediated mainly via the CLR-RAMP2 receptor complex.

Continuous administration of AM ameliorates pulmonary fibrosis

To assess the therapeutic effect of exogenously administered AM on pulmonary fibrosis, WT mice were administered BLM and then continuously infused with AM for 3, 7 or 14 days using an osmotic pump. With AM treatment, mice tended to have lighter lungs, although the effect was not significant (Supplementary Figure 7A-C). Gene expression analysis showed that expression of pro-inflammatory cytokines during the acute phase was suppressed in AM-treated mice (Supplementary Figure 7D, E), as was expression of fibrosis-related factors during the chronic phase (Supplementary Figure 7F). Similarly, pathological analysis showed that both inflammatory cell infiltration during the acute phase and fibrosis during the chronic phase were suppressed in AM-treated mice as compared to saline-treated mice (Supplementary Figure 8A-H). These results suggest that, like endogenous AM, exogenously administered AM suppresses the pathogenesis of

pulmonary fibrosis and that continuous administration of AM would be an effective mean of treating pulmonary fibrosis.

TGF-β-signaling is enhanced during pulmonary fibrosis in AM+/- mice

Earlier studies suggest that the transforming growth factor-β (TGF-β)-Smads pathway is involved in the process of BLM-induced pulmonary fibrosis (19,61,62). To explore the mechanism of the antifibrotic effect of AM, we focused on TGF-β and its intracellular signaling during the chronic phase (days 14 and 28) after BLM administration. The lungs of BLM-administered mice showed increased expression of the gene encoding TGF-β1 (*Tgfb1*), but there was no significant difference between AM+/- and WT mice (Figure 4A). On the other hand, activation of Smad3, a downstream mediator of TGF-β1 signaling, was significantly enhanced in AM+/- lungs on days 14 and 28 after BLM administration compared with WT mice (Figure 4B). Similarly, activation of Smad2 also tended to be upregulated in AM+/- mice, though the effect was not significantly different from that in WT mice (Figure 4C).

Stimulation of AM+/- fibroblasts with TGF-β results in the appearance of larger myofibroblasts

We next examined the effects of TGF-β on primary cultures of fibroblasts collected from the lungs of AM+/- and WT mice that had not been administered BLM. Figure 5A shows the results of immunostaining the primary lung fibroblasts. We also quantified the α-SMA-positive cell fraction (Figure 5B) and measured their size (Figure 5C). In Figure 5B, the ratio of α-SMA-positive to vimentin-positive cells (α-SMA / vimentin) indicates the percentage of myofibroblasts among the primary mesenchymal cells (mostly fibroblasts). Compared with WT, cells cultured from AM+/- lungs tended to have a higher proportion of myofibroblasts that were positive for α-SMA immunostaining (Figure 5B, control). In addition, α-SMA-positive myofibroblasts from AM+/- lungs tended to be larger in size, even when unstimulated (Figure 5C, control). Among the cells from WT lungs, the number of α-SMA-positive myofibroblasts increased after TGF-β-stimulation, though the change was not significant (Figure 5B, compare white columns between control and TGF-β1). These cells also tended to be enlarged (Figure 5C, compare white columns between control and TGF-β1). Among the cells from AM+/- lungs, the increase

in α-SMA-positive cells (Figure 5B, compare black columns between control and TGF-β1) and their cellular enlargement (Figure 5C, compare black columns between control and TGF-β1) were made much more pronounced by TGF-β stimulation. Notably, however, the TGF-β-induced changes observed in AM+/- cells were canceled by application of AM to the cells (Figure 5B and Figure 5C, compare black columns between TGF-β1 and TGF-β1+AM). These results indicate that under conditions where AM levels are decreased while TGF-β levels are increased, the numbers of α-SMA-positive myofibroblasts are increased and the cells are larger.

Comparison of the proliferative and migratory capacities of TGF-β-stimulated AM+/- and WT cells revealed that the proliferative capacity of AM+/- cells was significantly lower than that of WT cells (Figure 6A). Likewise, scratch assays showed that AM+/- cells had a significantly lower migratory capacity than WT cells (Figure 6B). These results suggest that when fibroblasts derived from the lungs of AM+/- mice are stimulated with TGF-β, they likely to differentiate into myofibroblasts characterized by larger size and lower proliferative and migratory capacities.

Stimulation of AM+/- fibroblasts with TGF-β increases nonproliferating myofibroblasts

Given the findings in the previous section, we classified lung-derived cells based on their intracellular actin fiber formation, the presence or absence of α-SMA expression, and cell proliferation potential in addition to their morphology. As described previously (63), fluorescence microscopy was used to classify the cells into four types based on their actin fiber formation (phalloidin staining), α-SMA expression and proliferative potential (Ki-67 immunostaining) (Figure 7). Cells with mild actin fiber formation, no expression of α-SMA, and high proliferative potential were classified as fibroblasts (Fbs). Cells with actin fiber formation but no expression of α-SMA and high proliferative potential were classified as proto-myofibroblasts (proto-MyoFbs). Cells with high proliferative potential and both actin fiber formation and α-SMA expression were classified as proliferating myofibroblasts (p-MyoFbs). And cells with actin fiber formation and α-SMA expression but without proliferative capacity were classified as nonproliferating myofibroblasts (non-p-MyoFbs) (Figure 7). Cells that could not be classified based on immunostaining were excluded from the counting; about 70-80% of the cells examined were classified

into these 4 types. Figure 8 shows the Fb (Figure 8A), proto-MyoFb (Figure 8B), p-MyoFb (Figure 8C) and non-p-MyoFb (Figure 8D) fractions expressed as percentages of the total classified cells. Only after stimulation with TGF-β1 were there significant differences in the percentages of each cell type between AM+/-−derived and WT-derived cells. In other words, TGF-β1 stimulation of AM+/- lung-derived fibroblasts led to a decrease in cells classified as p-MyoFbs (Figure 8B) and an increase in cells classified as non-p-MyoFbs (Figure 8D). On the other hand, the change in cell profile (decrease of p-MyoFbs and increase of non-p-MyoFbs) observed among TGF-β1-stimulated AM+/- derived cells was blocked when AM was applied to the cells (Figure 8B, C, TGF-β1 + AM).

We also immunostained AM+/- and WT lung specimens to determine how the cell profiles in the lung had changed 14 days after BLM administration. The results showed that numbers of p-MyoFbs (α-SMA (+), Ki67 (+)) were decreased and non-p-MyoFb (α-SMA (+), Ki67 (-)) were increased in AM+/- lungs after BLM administration (Supplementary Figure 9), which is consistent with the *in vitro* study (Figure 8).

Nonproliferating myofibroblasts are highly productive and contractile

To further investigate the cells classified as non-p-MyoFbs, we examined the characteristics of TGF-β1-stimulated AM+/- cells. We found that expression of the genes encoding type I collagen α1 (*Col1a1*), a central component of extracellular matrix, TIMP-1 (*Timp-1*), a suppressor of collagen degradation, and MCP-1 (*Ccl2*), a chemoattractant of inflammatory cells, were all significantly upregulated in TGF-β1-stimulated AM+/- cells (Figure 9A-C). These gene expression changes were cancelled when AM was added. On the other hand, expression of the gene encoding Meflin (*ISlr*), a recently discovered marker of steady-state fibroblasts (64,65), was greatly reduced in both AM+/- and WT cells upon stimulation with TGF-β1 (Figure 9D). The marked downregulation of *ISlr* by TGF-β1 was not reversed when AM was added.

As the differentiated myofibroblasts exhibited higher levels of actin filaments, some of which were α-SMA-positive, we examined their ability to contract within a three-dimensional collagen matrix (Figure 10A). AM+/- and WT cells both contracted upon TGF-β1-stimulation, but the contractions were significantly greater in AM+/- cells (Figure 10B, TGF-β1). These TGF-β1-induced contractions were also canceled by

application of AM (Figure 10B, TGF-β1 + AM).

Collectively, these findings indicate that non-p-MyoFbs are larger in size, have lower capacities for proliferation and migration, but higher capacities for filamentous actin formation, contraction, and production of extracellular matrix and chemoattractant for recruitment of inflammatory cells.

TGF-β downstream signaling is activated in nonproliferating myofibroblasts

Because TGF-β signaling was more activated in the lungs of BLM-administered AM+/- mice than WT mice, we investigated whether it was more activated in TGF-β-stimulated AM+/- fibroblasts than WT fibroblasts. In the absence of stimulation, the activation levels of Smad2 and Smad3, two downstream TGF-β signaling molecules, did not differ between AM+/- and WT cells (Figure 11A and 11B, control). By contrast, when stimulated with TGF-β, AM+/- cells showed a significantly greater increase in Smad3 activation than WT cells (Figure 11A, TGF-β1), but that effect was suppressed by application of AM (Figure 11A, TGF-β1 + AM). Smad2 activation tended to increase when AM+/- cells were stimulated with TGF-β, but the effect did not significantly differ from WT cells (Figure 11B, TGF-β).

Those results suggest that TGF-β and its downstream signaling molecules are involved in the differentiation of AM+/- lung-derived fibroblasts into non-p-MyoFbs. To further test that idea, we examined how non-p-MyoFbs were effected by treatment with SB431542, a selective TGF-β receptor-1 (TGFβR1) inhibitor, or SIS3, a Smad3-selective inhibitor (Figure 12A). We found that treatment with SB431542 or SIS3 reduced the increase in non-p-MyoFb seen when AM+/- cells were stimulated with TGF-β and eliminated the significant difference between AM+/- and WT cells (Figure 12B, C). The effect of these TGF-β signaling inhibitors (SB431542 or SIS3) on the appearance of non-p-MyoFbs was similar to the effect of external AM seen in Figure 5.

Smad7 expression is downregulated in AM+/- lungs and TGF-β-stimulated AM+/- fibroblasts after BLM administration

Unlike Smad2 and Smad3, two receptor-activated Smads (R-Smads), Smad7, an antagonistic Smad, stably binds to TGFβR1, thereby suppressing activation of Smad2, Smad3 and TGF-β signaling. We found that Smad7 expression was significantly

downregulated in the lungs of AM+/- mice compared to WT mice, both in the controls (Figure 13A, control) and 14 days after BLM administration (Figure 13A, Day14). Furthermore, Smad7 expression was also significantly downregulated in TGF-β-stimulated AM+/- cells as compared to WT cells (Figure 13B, TGF-β). However, when AM was added, the downregulation of Smad7 was reversed (Figure 13B, TGF-β+AM). In addition, treating WT cells with AM alone significantly upregulated Smad7 expression (Figure 13C), which may in turn suppress TGF-β-Smad3 signaling.

miR-21 expression was upregulated in BLM-administered AM+/- lungs and TGF-β-stimulated AM+/- fibroblasts

It is now apparent that microRNAs are involved in a wide variety of pathophysiological processes, including pulmonary fibrosis. Among them, we focused on the pro-fibrotic miR-21, encoded by *Mir21* (66). In control lungs, there was no difference in the expression of miR-21between AM+/- and WT mice (Figure 14A, control). However, BLM-administration resulted in a significant elevation in miR-21 expression in AM+/- mice on day 14 (Figure 14A, Day 14). WT mice also showed the tendency toward elevated miR-21 expression after BLM administration; however, the effect was not statistically significant, leading to a significant difference between AM+/- and WT mice on day 14 (Figure 14A, Day14). The upregulated miR-21 expression declined to control levels by day 28 (Figure 14A, Day 28).

To confirm whether miR-21 expression is related to myofibroblast differentiation, we also examined its expression in the fibroblasts derived from AM+/- and WT lungs and compared its expression with and without TGF-β and AM administration (Figure 14B). In the absence of TGF-β1, miR-21 expression did not differ between AM+/- and WT cells with or without AM administration (Figure 14B, TGF-β1(-)). By contrast, upon stimulation with TGF-β1, miR-21 expression was upregulated to a significantly greater degree in AM+/- cells than WT cells (Figure 14B, TGF-β1(+), AM(-)). When AM was added in addition to TGF-β1, the difference in miR-21 expression between AM+/- and WT cells was eliminated (Figure 14B, TGF-β1(+), AM(+)). Taken together, these results suggest that 1) administering BLM to WT mice or stimulating WT cells with TGF-β1 elicit only small, non-significant changes in miR-21 expression; 2) miR-21 expression in both AM+/- and WT cells is unaffected by AM alone; and 3) only BLM-administered

AM+/- mice and TGF-β1-stimulated AM+/- cells show significant upregulation of miR-21 expression. Thus, miR-21 is significantly upregulated in myofibroblasts only when TGF-β levels are increased with a simultaneous decrease in AM levels.

Downregulation of miR-21 in TGF-β-stimulated AM+/- cells suppresses the differentiation of nonproliferating myofibroblasts

To confirm the involvement of miR-21 in the differentiation of non-p-MyoFbs, we next assessed the effect of a miR-21 inhibitor on the differentiation of TGF-β-stimulated AM+/- and WT fibroblasts (Figure 15). Application of the miR-21 inhibitor to the cells significantly reduced the number of large α-SMA-positive myofibroblasts (i.e., non-p-MyoFbs among AM+/-). These results indicate that miR-21 is a regulator of non-p-MyoFb differentiation through activation of TGF-β signaling in AM+/- cells.

Discussion

In the present study, we used a mouse BLM-induced pulmonary fibrosis model to investigate the pathophysiological significance of the AM-RAMP2 system. Both AM+/- and RAMP2+/- mice showed exacerbation of pulmonary fibrosis. In AM+/- and RAMP2+/- mice, marked inflammation in the lungs was observed during the acute phase after BLM administration. This was followed by marked fibrosis during the chronic phase. Kach et al. reported that transgenic mice overexpressing RAMP2 under the control of the α-SMA promoter had improved survival and reduced pulmonary fibrosis in the BLM model (41). Their results mirror those of our AM+/- or RAMP2+/- mice and support the idea that the AM-RAMP2 system acts as an inhibitory mediator in the pathogenesis of pulmonary fibrosis.

The TGF-β-Smads pathway is known to be a major cause of fibrosis. Within the lungs of AM+/- mice administered BLM, the activation level of Smad3, a receptor-activated Smad, was increased. Expression of *Tgfb1*, the gene encoding TGF-β1, was also upregulated by BLM administration, though the expression level did not significantly differ between WT and AM+/- mice. These observations suggest that in AM+/-, BLM administration does not increase *Tgfb1* expression itself, but instead enhances the activation of downstream mediators of TGF-β. On the other hand, activation of Smad2, another receptor-activated Smad, was not significantly changed in AM+/- as compared to WT. Although Smad2 is structurally highly similar to Smad3, and both Smad2 and Smad3 are directly phosphorylated by TGFβR1, a receptor tyrosine kinase, they do not share similar DNA-binding activity (67). Gu et al. reported that it is Smad3, not Smad2, that functions as the major mediator of TGF-β1 signaling to activate *Acta2* (α-SMA) gene expression in vitro (68). That result was confirmed in Smad3 knockout mice, which showed attenuated lung fibrosis after BLM administration (67). In the present study, we also found a clear and significant difference in the levels of Smad3 activation between AM+/- and WT cells after TGF-β stimulation. These observations suggest that TGFβR1 and Smad3 activation are important downstream TGF-β signals involved in exacerbating pulmonary fibrosis in AM+/- mice. This was also confirmed by the experiments using a TGFβR1 or Smad3 inhibitor, both of which suppressed the effect of TGF-β.

Fibroblasts are the major mesenchymal cells in the lung, and differentiation from fibroblasts to myofibroblasts is a key event in the process of fibrosis (69). When

inflammatory stimuli persist, fibroblasts differentiate into myofibroblasts, which exhibit enhanced extracellular matrix production. The resultant acceleration of extracellular matrix deposition leads to the development of fibrosis (43). TGF-β is a potent inducer of differentiation to α-SMA-positive myofibroblasts (MyoFbs) (70). In the present study, TGF-β-stimulated α-SMA-positive MyoFbs derived from AM+/- mice showed reduced proliferative and migratory potentials. These cells were also larger in size and exhibited enhanced contractility. Driesen, et al. reported that TGF-β promotes differentiation of proliferating MyoFbs (p-MyoFbs) to MyoFbs which exhibit a near absence of proliferation and named them nonproliferating-MyoFbs (non-p-MyoFbs) (71). Non-p-MyoFbs produce large amounts of collagen and chemoattractant molecules that recruit inflammatory cells. In the present study, we also found that TGF-β-stimulated AM+/- cells exhibited higher expression of collagen, TIMP1 and MCP-1 than WT cells. TIMP1 inhibits degradation of extracellular matrix by inactivating matrix metalloproteinases. MCP-1 acts as a migratory factor for monocytes and is associated with chronic inflammation. These results suggest that non-p-MyoFbs, which were increased among TGF-β-stimulated AM+/- cells, are deeply involved in the exacerbation of pulmonary fibrosis. These properties of non-p-MyoFbs were suppressed by adding AM to TGF-β-stimulated AM+/- cells. By contrast, expression of Meflin, a recently discovered marker of steady-state fibroblasts (64,65), was downregulated by the TGF-β stimulation, but that effect was not reversed by AM treatment. This suggests AM can suppress TGF-β-induced differentiation of p-MyoFbs to non-p-MyoFbs, but it cannot return them to normal steady state fibroblasts.

It is now clear that dysregulation of microRNAs is linked to a wide variety of diseases, including fibrosis of the liver (72), kidney (73), heart (74) and lung (66). MicroRNAs work as regulators of gene expression, and some have also attracted attention as regulators of the TGF-β-Smads pathway and fibrosis (66). Among them, we focused on miR-21, encoded by *Mir21*, levels of which are reportedly elevated in the lungs of pulmonary fibrosis patients and BLM-administered mice (75). Furthermore, the enhanced *Mir21* expression is primarily localized in myofibroblasts, where its product, miR-21, activates them to promote the progression of fibrosis (75). The profibrotic properties of miR-21 are thought to be mediated via downregulation of Smad7, an inhibitor of the TGF-β-Smads pathway. Indeed, Smad7 is reported to be a direct target of miR-21 in

various diseases including pulmonary fibrosis, renal fibrosis and cancers (66,73,76). In the present study, we were able to confirm that *Mir21* expression is upregulated, while Smad7 expression is downregulated, in the lungs of AM+/- mice administered BLM. In our *in vitro* experiments, we also found that *Mir21* expression is highly upregulated only when AM+/- cells are stimulated with TGF-β and that addition of AM cancels that effect. These observations suggest that AM works to suppress TGF-β-evoked *Mir21* expression and upregulate Smad7 expression. We also confirmed that the effects of inhibiting miR-21 on the differentiation of p-MyoFbs to non-p-MyoFbs were similar to those of AM or TGF-β-Smad3 inhibitors.

Figure 16 summarizes our findings on the effects of the AM-RAMP2 system in the pathogenesis of pulmonary fibrosis. In addition to suppressing inflammation during the early phase, the AM-RAMP2 system also suppresses fibrosis progression by regulating miR-21 expression, the TGF-β-Smads pathway, and non-p-MyoFb differentiation during the chronic phase. These results indicate that the AM-RAMP2 system suppresses the progression of pulmonary fibrosis, making it a promising new target for the treatment of pulmonary fibrosis, for which there are currently limited therapeutic options.

In the treatment of pulmonary fibrosis, pirfenidone and nintedanib are two newer drugs that have recently come into use (77). The primary mechanism of action of pirfenidone is inhibition of TGF-β production and suppression of differentiation of type 2 alveolar epithelial cells into fibroblasts and myofibroblasts. Nintedanib is a small molecule tyrosine kinase inhibitor that acts on the vascular endothelial growth factor receptor (VEGFR), fibroblast growth factor receptor (FGFR), and platelet-derived growth factor receptor (PDGFR). So far, these drugs have not proved adequately effective and have several adverse side effects. In the context of fibrosis, AM suppresses both inflammation and fibrosis. In addition, because AM is an endogenous bioactive peptide, it is expected to be a safer therapeutic agent than steroids, immunosuppressive agents, anti-inflammatory drugs and the two aforementioned antifibrotic drugs. However, the indications for AM are limited due to its short half-life; AM treatment would require continuous intravenous infusion under hospitalization. In that context, RAMP2 could be an alternative therapeutic target for AM.

Figure legends

Figure 1

Bleomycin-induced pulmonary fibrosis is more severe in AM+/- mice

A: Appearance of the lungs from control and bleomycin-administered AM+/- and WT mice (Day 14). **B:** Lung weight ratios. The mean of the WT control group was assigned a value of 1 (n=6-14). **C:** Lung weight / body weight (mg/g) ratios (n=6-14). **D:** Hydroxyproline levels in the lungs of AM+/- and WT mice (n=5). **E, F:** Quantitative real-time PCR analysis of inflammation-related genes (n=5). **G-J:** Quantitative real-time PCR analysis of fibrosis-related genes (n=5-6). In **E-J,** the means of the WT control groups were assigned a value of 1. Bars are means ± SEM. "*" indicates comparison between the groups, "#" indicates comparison with WT control, "†" indicates comparison with AM+/- control. p-values were calculated using two-way ANOVA with Tukey's test.

Figure 2

Pathology of bleomycin-induced inflammation and fibrosis in lungs of AM+/- mice

A, B: Representative photomicrographs of lung tissues stained with hematoxylin / eosin (H&E) or Masson's trichrome (MT) or immunostained for α-smooth muscle actin (α-SMA) on day 14 after bleomycin treatment (**A**) and immunostaining for CD45, F4/80 or CD3 on day 7 after bleomycin treatment (**B**). **Left column:** WT lungs, **Right column:** AM+/- lungs. Scale bars with H&E and MT staining = 100 μm. Scale bars with α-SMA, CD45, F4/80 and CD3 immunostaining = 50 μm. **C:** Modified Ashcroft score quantifying pulmonary fibrosis (n=5-9). **D:** Percentage of the Masson's trichrome stained fibrotic area / HPF (400x) (n=5). **E:** Percentage of α-SMA-positive area / HPF (400x) (n=5-9). **F-H**: Numbers of CD45-positve leukocytes (**F**), F4/80-positive macrophages (**G**) and CD3-positive T cells (**H)** / HPF (400x) (n=4-11). Bars are means ± SEM. "*" indicates comparison between the groups, "#" indicates comparison with WT control, "†" indicates comparison with AM+/- control. p-values were calculated using two-way ANOVA with Tukey's test.

Figure 3

Changes of inflammatory cell populations during bleomycin-induced pulmonary fibrosis in AM+/- mice

A-C: Flow cytometric analysis of lung inflammation in AM+/- and WT mice after treatment with bleomycin. **A**: Eosinophils (SiglecF+CD11b+ in CD45+CD11c–Ly6G–). **B:** Monocytes (Ly6C+CD11b+ in CD45+CD11c–Ly6G–SiglecF–). **C:** Neutrophils (Ly6G+CD11b+ in CD45+CD11c–). Numbers indicate the percentage of the cell population in each plot. Gating was performed as shown in Supplementary Figure 1. **D:** Absolute numbers of eosinophils, monocytes and neutrophils in lungs from mice left untreated or treated with bleomycin (n=4-6). Bars are means ± SEM. "*" indicates comparison between the groups, "#" indicates with comparison with WT control, "†" indicates comparison with AM+/- control. p-values were calculated using Two-way ANOVA with Tukey's test.

Figure 4

TGF-β-signaling is enhanced in bleomycin-administered AM+/- mice

A: Quantitative real-time PCR analysis of *Tgfb1* expression 14 and 28 days after bleomycin administration to AM+/- and WT mice. The mean of the WT control was assigned a value of 1 (n=5). Bars are means ± SEM. **B, C: Upper row:** Representative Western blots of Smad3 and p-Smad3 (**B**) and Smad2 and p-Smad2 (**C**) in AM+/- and WT lungs left untreated (control) and on days 14 and 28 after bleomycin administration. β-actin was used as a loading control. **B, C: Lower row:** Levels of Smad2 and Smad3 activation as indicated by band intensity ratios (p-Smad2 / Smad2 and p-Smad3 / Smad3) Means of WT controls were assigned a value of 1 (n=3-4). Bars are means ± SEM. "*" indicates compared between the groups, "#" indicates comparison with WT control, "†" indicates comparison with AM+/- control. p-values were calculated using two-way ANOVA with Tukey's test.

Figure 5

TGF-β1-induced differentiation of fibroblasts to myofibroblasts and its suppression by AM

A: Representative images of immunostained (Green: α-SMA, Red: vimentin, Blue: DAPI) primary cultured fibroblasts isolated from the lungs of AM+/- and WT mice.

Cells were grown to 70% confluence. Immunostaining was performed in control cells and cells pretreated with AM (10^{-7} M) or PBS for 2 h and then stimulated with TGF-β1 (10 ng/mL) for 24 h. Scale bars = 100 μm. **B:** Percentage of α-SMA-positive area / vimentin-positive area. **C:** Size of α-SMA-positive cells (**B, C**). Data are from 3 independent experiments. Bars are means ± SEM. "*" indicates comparison between the groups, "†" indicates comparison with AM+/- control. p-values were calculated using two-way ANOVA with Tukey's test.

Figure 6

Cell proliferation and migration is reduced in primary cultured AM+/- lung fibroblasts stimulated with TGF-β

A: Cell proliferation was assessed using a cell counting kit with water-soluble tetrazolium salt as a substrate. Data are shown as the ratio of cell proliferation when the mean of the WT cells was assigned a value of 1 (n = 4). **B:** Cell migration was assessed using scratch assays. **Upper row:** Representative photomicrographs showing the status of the scratch in a cultured cell monolayer 0 h and 6 h after scratching. Scale bars = 200 μm. **Lower row:** The cell migration distance was calculated from change in the width of the scratch between 0 h and 6 h. The data are from 3 independent experiments. Bars are means ± SEM. "*" indicates comparison between the groups. p-values were calculated using Student's t test.

Figure 7

Classification of the lung fibroblasts stimulated with TGF-β

Shown are phalloidin staining, DAPI staining, and immunostaining for α-SMA and Ki67 in representative cells in each indicated category. Cells with mild actin fiber formation, no expression of α-SMA, and high proliferative potential (F-actin (+/-), α-SMA (-), Ki-67 (+)) were defined as fibroblasts (Fbs). Cells with actin fiber formation but no expression of α-SMA and high proliferative capacity (F-actin (+), α-SMA (-), Ki-67 (+)) were defined as proto-myofibroblasts (proto-MyoFbs). Cells with high proliferative potential, which showed both actin fiber formation and expression of α-SMA (F-actin (+), α-SMA (+), Ki-67 (+)) were defined as proliferating-myofibroblasts (p-MyoFbs). Cells with actin fiber formation and α-SMA expression but lost proliferative capacity (F-actin

(+), α-SMA (+), Ki-67 (-)) were defined as nonproliferating-myofibroblasts (non-p-MyoFbs). Scale bars = 20 μm.

Figure 8

Stimulation of AM+/- fibroblasts with TGF-β increases nonproliferating myofibroblasts

A-D: AM+/- and WT lung fibroblasts were classified into 4 categories (**A:** fibroblasts (Fbs), **B:** proto-myofibroblasts (proto-MyoFbs), **C:** proliferating-myofibroblasts (p-MyoFbs) and **D:** nonproliferating-myofibroblasts (non-p-MyoFbs)) based on cell staining. Shown are their percentages among the control, TGF-β1-stimulated and TGF-β1-stimulated + AM groups. Data are from 3 independent experiments. Bars are means ± SEM. "*" indicates comparison between the groups. p-values were calculated using two-way-ANOVA with Tukey's test.

Figure 9

TGF-β-stimulated AM+/- fibroblasts show upregulation of genes related to fibrosis and inflammation but downregulation of a steady-state fibroblast marker

A-D: Quantitative real-time PCR analysis of *Col1a1* (Type Ⅰ collagen α1) (**A**), *Timp1* (TIMP-1) (**B**), *Ccl2* (MCP-1) (**C**) and *Islr* (Meflin) (**D**) in AM+/- and WT lung fibroblasts. The means of the WT control group were assigned a value of 1 (n=5). Bars are means ± SEM. "*" indicates comparison between the groups, "#" indicates comparison with WT control, "#" indicates comparison with WT control, "†" indicates comparison with AM+/- control. p-values were calculated using two-way ANOVA with Tukey's test.

Figure 10

TGF-β-stimulated AM+/- fibroblasts show enhanced contractility

A: Representative images of culture dishes in a gel contraction assay. **A:** "Contracture rings" (white dotted circles) show the borders of the measured area 12 h after gel release. Scale bars = 5 mm. **B:** Relative gel area 12 h after collagen gel release from the well's wall. A smaller gel area indicates greater cellular contraction. The mean of the WT control group was assigned a value of 1. Data are from 3 independent experiments. Bars are

means ± SEM. "*" indicates comparison between the groups, "#" indicates comparison with WT control, "†" indicates comparison with AM+/- control. p-values were calculated using two-way ANOVA with Tukey's test.

Figure 11

TGF-β-stimulated AM+/- fibroblasts show greater Smad3 activation

A, B: Upper row: Representative Western blots showing expression of Smad3 and phosphorylated (p)-Smad3 (**A**) and Smad2 and p-Smad2 (**B**) in AM+/- and WT lung fibroblasts (control and TGF-β1-stimulated cells with or without AM-treatment). β-actin was used as a loading control. **A, B: Lower row:** p-Smad3 / Smad3 (**A**) and p-Smad2 /Smad2 (**B**) band density ratios showing the level of Smad3 (**A**) and Smad2 (**B**) activation. Means of WT controls were assigned a value of 1. Data are from 4 independent experiments. Bars are means ± SEM. "*" indicates comparison between the groups, "#" indicates comparison with WT control, "†" indicates comparison with AM+/- control. p-values were calculated using two-way ANOVA with Tukey's test.

Figure 12

TβRI or Smad3 inhibition suppresses the occurrence of nonproliferating myofibroblasts (non-p-MyoFbs) among TGF-β-stimulated AM+/- fibroblasts

A: Representative images of immunostained (Green: α-SMA, Red: vimentin, Blue: DAPI) primary cultured lung fibroblasts isolated from AM+/- and WT mice. The cells were grown to 70% confluence. Immunostaining was performed in control cells and in cells stimulated with TGF-β1 (10 ng/mL) for 24 h with or without SB431542 (10 μM), an inhibitor of TGF-β type I receptor (TGFβRI) or SIS3 (3 μM), an inhibitor of Smad3. Scale bars = 100 μm. **B:** Percentage α-SMA-positive area / vimentin-positive area. **C:** Size of α-SMA-positive cells. Data are from 3 independent experiments. Bars are means ± SEM. "*" indicates comparison between the groups, "#" indicates comparison with WT control, "†" indicates comparison with AM+/- control. p-values were calculated using two-way ANOVA with Tukey's test.

Figure 13

Expression of Smad7 is downregulated in AM+/- but is restored by AM treatment

A, B: Upper row: Representative Western blots showing expression of Smad7 in lungs from AM+/- and WT mice left untreated (control) and 14 and 28 days after bleomycin administration (**A**) and in AM+/- and WT lung fibroblasts (control cells and TGF-β1-stimulated cells with or without AM-treatment) (**B**). β-actin was used as a loading control. **A, B: Lower row:** Relative levels of Smad7 expression determined from the corresponding band densities. The means of the WT controls were assigned a value of 1 (n=3-4). Bars are means ± SEM. "*" indicate comparison between the groups, "#" indicates comparison with WT control, "†" indicates comparison with AM+/- control. p-values were calculated using two-way ANOVA with Tukey's test. **C: Upper row:** Representative Western blots showing expression of Smad7 in WT lung fibroblasts with or without 10^{-7} M AM for 24 h. β-actin was used as a loading control. **C: Lower row:** Relative levels of Smad7 expression determined from the corresponding band densities. The mean of the WT control was assigned a value of 1 (n=3). Bars are means ± SEM. "*" indicates comparison between the groups. p-value was calculated using Student's t test.

Figure 14

Expression of miR-21 is upregulated in bleomycin-administered AM+/- mice and TGF-β-stimulated AM+/- fibroblasts

A: Quantitative real-time PCR analysis of microRNA-21 (miR-21) in AM+/- and WT mice left untreated (control) and 14 and 28 days after bleomycin administration. The mean of the WT control was assigned a value of 1 (n=5). Bars are means ± SEM. "*" indicates comparison between the groups, "†" indicates comparison with AM+/- control. **B:** Quantitative real-time PCR analysis of miR-21 in AM+/- and WT lung fibroblasts. The mean of the WT control (TGF-β (-), AM (-)) group was assigned a value of 1 (n=5). Bars are means ± SEM. "*" indicates comparison between the groups, "†" indicates comparison with AM+/- control (TGF-β (-), AM (-)). p-values were calculated using two-way ANOVA with Tukey's test.

Figure 15

microRNA-21 inhibition suppresses the occurrence of non-p-MyoFbs among TGF-β-stimulated AM+/- fibroblasts

A: Representative images of immunostained (Green: α-SMA, Red: vimentin, Blue:

DAPI) primary cultured lung fibroblasts isolated from the lungs of AM+/- and WT mice. The cells were grown to 70% confluence. Immunostaining was performed with control and TGF-β1-stimulated (10 ng/mL for 24 h) cells with or without miR-21 inhibitor. Scale bars = 100 μm. **B:** Percentage α-SMA-positive area / vimentin-positive area. **C:** Size of α-SMA-positive cells. Data are from 3 independent experiments. (**B, C**). Bars are means ± SEM. "*" indicates comparison between the groups, "#" indicates comparison with WT control, "†" indicates comparison with AM+/- control. p-values were calculated using two-way ANOVA with Tukey's test.

Figure 16

Roles of the AM-RAMP2 system in the pathogenesis of pulmonary fibrosis

During the pathogenesis of pulmonary fibrosis, the AM-RAMP2 system suppresses inflammation during the early acute phase. Later, during the chronic phase, AM-RAMP2 inhibits the progression of fibrosis by suppressing miR-21 expression, signaling in the TGF-β-Smads pathway, and differentiation to nonproliferating myofibroblasts (non-p-MyoFbs).

Acknowledgement

The authors are grateful to Dr. Shinsuke Taki for valuable comments and to Dr. Kenji Kangawa for providing human recombinant AM.

Data availability statement

Some or all data generated or analyzed during this study are included in this published article or Supplementary data linked this article.

References

1. Yamazaki R, Nishiyama O, Saeki S, Sano H, Iwanaga T, Tohda Y. Characteristics of patients with chronic idiopathic interstitial pneumonia undergoing repeated respiratory-related hospitalizations: A retrospective cohort study. PLoS One 2020; 15:e0232212
2. Disayabutr S, Calfee CS, Collard HR, Wolters PJ. Interstitial lung diseases in the hospitalized patient. BMC Med 2015; 13:245
3. Kitamura K, Kangawa K, Kawamoto M, Ichiki Y, Nakamura S, Matsuo H, Eto T. Adrenomedullin: a novel hypotensive peptide isolated from human pheochromocytoma. Biochem Biophys Res Commun 1993; 192:553-560
4. Ichiki Y, Kitamura K, Kangawa K, Kawamoto M, Matsuo H, Eto T. Distribution and characterization of immunoreactive adrenomedullin in human tissue and plasma. FEBS Lett 1994; 338:6-10
5. Michibata H, Mukoyama M, Tanaka I, Suga S, Nakagawa M, Ishibashi R, Goto M, Akaji K, Fujiwara Y, Kiso Y, Nakao K. Autocrine/paracrine role of adrenomedullin in cultured endothelial and mesangial cells. Kidney Int 1998; 53:979-985
6. Kitamura K, Ashizuka S, Inatsu H, Kita T. Adrenomedullin as a Potential Therapeutic Agent for Refractory Ulcerative Colitis. In: Nakao K, Minato N, Uemoto S, eds. Innovative Medicine: Basic Research and Development. Tokyo2015:227-240.
7. Ashizuka S, Kuroishi N, Nakashima K, Inatsu H, Kita T, Kitamura K. Adrenomedullin: A Novel Therapy for Intractable Crohn's Disease with a Loss of Response to Infliximab. Intern Med 2019; 58:1573-1576
8. Kita T, Kaji Y, Kitamura K. Safety, Tolerability, and Pharmacokinetics of Adrenomedullin in Healthy Males: A Randomized, Double-Blind, Phase 1 Clinical Trial. Drug Des Devel Ther 2020; 14:1-11
9. Shindo T, Kurihara Y, Nishimatsu H, Moriyama N, Kakoki M, Wang Y, Imai Y, Ebihara A, Kuwaki T, Ju KH, Minamino N, Kangawa K, Ishikawa T, Fukuda M, Akimoto Y, Kawakami H, Imai T, Morita H, Yazaki Y, Nagai R, Hirata Y, Kurihara H. Vascular abnormalities and elevated blood pressure in mice lacking adrenomedullin gene. Circulation 2001; 104:1964-1971

10. Niu P, Shindo T, Iwata H, Ebihara A, Suematsu Y, Zhang Y, Takeda N, Iimuro S, Hirata Y, Nagai R. Accelerated cardiac hypertrophy and renal damage induced by angiotensin II in adrenomedullin knockout mice. Hypertens Res 2003; 26:731-736

11. Niu P, Shindo T, Iwata H, Iimuro S, Takeda N, Zhang Y, Ebihara A, Suematsu Y, Kangawa K, Hirata Y, Nagai R. Protective effects of endogenous adrenomedullin on cardiac hypertrophy, fibrosis, and renal damage. Circulation 2004; 109:1789-1794

12. Tanaka M, Kakihara S, Hirabayashi K, Imai A, Toriyama Y, Iesato Y, Sakurai T, Kamiyoshi A, Ichikawa-Shindo Y, Kawate H, Tanaka M, Cui N, Wei Y, Zhao Y, Aruga K, Yamauchi A, Murata T, Shindo T. Adrenomedullin-Receptor Activity-Modifying Protein 2 System Ameliorates Subretinal Fibrosis by Suppressing Epithelial-Mesenchymal Transition in Age-Related Macular Degeneration. Am J Pathol 2020;

13. Nishimatsu H, Hirata Y, Shindo T, Kurihara H, Kakoki M, Nagata D, Hayakawa H, Satonaka H, Sata M, Tojo A, Suzuki E, Kangawa K, Matsuo H, Kitamura T, Nagai R. Role of endogenous adrenomedullin in the regulation of vascular tone and ischemic renal injury: studies on transgenic/knockout mice of adrenomedullin gene. Circ Res 2002; 90:657-663

14. Shindo T, Kurihara H, Maemura K, Kurihara Y, Kuwaki T, Izumida T, Minamino N, Ju KH, Morita H, Oh-hashi Y, Kumada M, Kangawa K, Nagai R, Yazaki Y. Hypotension and resistance to lipopolysaccharide-induced shock in transgenic mice overexpressing adrenomedullin in their vasculature. Circulation 2000; 101:2309-2316

15. McLatchie LM, Fraser NJ, Main MJ, Wise A, Brown J, Thompson N, Solari R, Lee MG, Foord SM. RAMPs regulate the transport and ligand specificity of the calcitonin-receptor-like receptor. Nature 1998; 393:333-339

16. Shindo T, Tanaka M, Kamiyoshi A, Ichikawa-Shindo Y, Kawate H, Yamauchi A, Sakurai T. Regulation of cardiovascular development and homeostasis by the adrenomedullin-RAMP system. Peptides 2019; 111:55-61

17. Ichikawa-Shindo Y, Sakurai T, Kamiyoshi A, Kawate H, Iinuma N, Yoshizawa T, Koyama T, Fukuchi J, Iimuro S, Moriyama N, Kawakami H, Murata T, Kangawa

1052 K, Nagai R, Shindo T. The GPCR modulator protein RAMP2 is essential for
1053 angiogenesis and vascular integrity. J Clin Invest 2008; 118:29-39
1054 **18.** Koyama T, Ochoa-Callejero L, Sakurai T, Kamiyoshi A, Ichikawa-Shindo Y,
1055 Iinuma N, Arai T, Yoshizawa T, Iesato Y, Lei Y, Uetake R, Okimura A, Yamauchi
1056 A, Tanaka M, Igarashi K, Toriyama Y, Kawate H, Adams RH, Kawakami H,
1057 Mochizuki N, Martinez A, Shindo T. Vascular endothelial adrenomedullin-
1058 RAMP2 system is essential for vascular integrity and organ homeostasis.
1059 Circulation 2013; 127:842-853
1060 **19.** Cooper JA, Jr. Pulmonary fibrosis: pathways are slowly coming into light. Am J
1061 Respir Cell Mol Biol 2000; 22:520-523
1062 **20.** Murakami S, Nagaya N, Itoh T, Iwase T, Fujisato T, Nishioka K, Hamada K,
1063 Kangawa K, Kimura H. Adrenomedullin regenerates alveoli and vasculature in
1064 elastase-induced pulmonary emphysema in mice. Am J Respir Crit Care Med
1065 2005; 172:581-589
1066 **21.** Hobara N, Goda M, Kitamura Y, Sendou T, Gomita Y, Kawasaki H.
1067 Adrenomedullin facilitates reinnervation of phenol-injured perivascular nerves in
1068 the rat mesenteric resistance artery. Neuroscience 2007; 144:721-730
1069 **22.** Uetake R, Sakurai T, Kamiyoshi A, Ichikawa-Shindo Y, Kawate H, Iesato Y,
1070 Yoshizawa T, Koyama T, Yang L, Toriyama Y, Yamauchi A, Igarashi K, Tanaka
1071 M, Kuwabara T, Mori K, Yanagita M, Mukoyama M, Shindo T. Adrenomedullin-
1072 RAMP2 system suppresses ER stress-induced tubule cell death and is involved in
1073 kidney protection. PLoS One 2014; 9:e87667
1074 **23.** Imai A, Toriyama Y, Iesato Y, Hirabayashi K, Sakurai T, Kamiyoshi A, Ichikawa-
1075 Shindo Y, Kawate H, Tanaka M, Liu T, Xian X, Zhai L, Dai K, Tanimura K, Liu
1076 T, Cui N, Yamauchi A, Murata T, Shindo T. Adrenomedullin Suppresses Vascular
1077 Endothelial Growth Factor-Induced Vascular Hyperpermeability and
1078 Inflammation in Retinopathy. Am J Pathol 2017; 187:999-1015
1079 **24.** Hirabayashi K, Tanaka M, Imai A, Toriyama Y, Iesato Y, Sakurai T, Kamiyoshi A,
1080 Ichikawa-Shindo Y, Kawate H, Tanaka M, Dai K, Cui N, Wei Y, Nakamura K,
1081 Iida S, Matsui S, Yamauchi A, Murata T, Shindo T. Development of a Novel
1082 Model of Central Retinal Vascular Occlusion and the Therapeutic Potential of the
1083 Adrenomedullin-Receptor Activity-Modifying Protein 2 System. Am J Pathol

2019; 189:449-466

25. Eitzman DT, McCoy RD, Zheng X, Fay WP, Shen T, Ginsburg D, Simon RH. Bleomycin-induced pulmonary fibrosis in transgenic mice that either lack or overexpress the murine plasminogen activator inhibitor-1 gene. J Clin Invest 1996; 97:232-237

26. RRID:AB_2562562.

27. RRID:AB_2290801.

28. RRID:AB_2629529.

29. RRID:AB_2562414.

30. RRID:AB_2565852.

31. RRID:AB_1236488.

32. RRID:AB_2563054.

33. RRID:AB_10896143.

34. RRID:AB_10563422.

35. RRID:AB_1548790.

36. RRID:AB_394657.

37. RRID:AB_357485.

38. RRID:AB_323806.

39. RRID:AB_305055.

40. RRID:AB_2223500.

41. Hubner RH, Gitter W, El Mokhtari NE, Mathiak M, Both M, Bolte H, Freitag-Wolf S, Bewig B. Standardized quantification of pulmonary fibrosis in histological samples. Biotechniques 2008; 44:507-511, 514-507

42. RRID:AB_10626777.

43. RRID:AB_2193182.

44. RRID:AB_2193207.

45. RRID:AB_2889838.

46. RRID:AB_2889839.

47. RRID:AB_2223172.

48. Kono Y, Nishiuma T, Nishimura Y, Kotani Y, Okada T, Nakamura S, Yokoyama M. Sphingosine kinase 1 regulates differentiation of human and mouse lung fibroblasts mediated by TGF-beta1. Am J Respir Cell Mol Biol 2007; 37:395-404

49. Shimekake Y, Nagata K, Ohta S, Kambayashi Y, Teraoka H, Kitamura K, Eto T, Kangawa K, Matsuo H. Adrenomedullin stimulates two signal transduction pathways, cAMP accumulation and Ca2+ mobilization, in bovine aortic endothelial cells. J Biol Chem 1995; 270:4412-4417

50. Horio T, Kohno M, Kano H, Ikeda M, Yasunari K, Yokokawa K, Minami M, Takeda T. Adrenomedullin as a novel antimigration factor of vascular smooth muscle cells. Circ Res 1995; 77:660-664

51. Tanaka M, Koyama T, Sakurai T, Kamiyoshi A, Ichikawa-Shindo Y, Kawate H, Liu T, Xian X, Imai A, Zhai L, Hirabayashi K, Owa S, Yamauchi A, Igarashi K, Taniguchi S, Shindo T. The endothelial adrenomedullin-RAMP2 system regulates vascular integrity and suppresses tumour metastasis. Cardiovasc Res 2016; 111:398-409

52. Kang JH, Jung MY, Choudhury M, Leof EB. Transforming growth factor beta induces fibroblasts to express and release the immunomodulatory protein PD-L1 into extracellular vesicles. FASEB J 2020; 34:2213-2226

53. Jinnin M, Ihn H, Tamaki K. Characterization of SIS3, a novel specific inhibitor of Smad3, and its effect on transforming growth factor-beta1-induced extracellular matrix expression. Mol Pharmacol 2006; 69:597-607

54. RRID:AB_10562134.

55. RRID:AB_443209.

56. Bravo DD, Chernov-Rogan T, Chen J, Wang J. An impedance-based cell contraction assay using human primary smooth muscle cells and fibroblasts. J Pharmacol Toxicol Methods 2018; 89:47-53

57. Iesato Y, Toriyama Y, Sakurai T, Kamiyoshi A, Ichikawa-Shindo Y, Kawate H, Yoshizawa T, Koyama T, Uetake R, Yang L, Yamauchi A, Tanaka M, Igarashi K, Murata T, Shindo T. Adrenomedullin-RAMP2 system is crucially involved in retinal angiogenesis. Am J Pathol 2013; 182:2380-2390

58. Liu Y, Li Y, Li N, Teng W, Wang M, Zhang Y, Xiao Z. TGF-beta1 promotes scar fibroblasts proliferation and transdifferentiation via up-regulating MicroRNA-21. Sci Rep 2016; 6:32231

59. Swaisgood CM, French EL, Noga C, Simon RH, Ploplis VA. The development of bleomycin-induced pulmonary fibrosis in mice deficient for components of the

fibrinolytic system. Am J Pathol 2000; 157:177-187

60. Koyama T, Sakurai T, Kamiyoshi A, Ichikawa-Shindo Y, Kawate H, Shindo T. Adrenomedullin-RAMP2 System in Vascular Endothelial Cells. J Atheroscler Thromb 2015; 22:647-653

61. Giri SN, Hyde DM, Hollinger MA. Effect of antibody to transforming growth factor beta on bleomycin induced accumulation of lung collagen in mice. Thorax 1993; 48:959-966

62. Wang Q, Wang Y, Hyde DM, Gotwals PJ, Koteliansky VE, Ryan ST, Giri SN. Reduction of bleomycin induced lung fibrosis by transforming growth factor beta soluble receptor in hamsters. Thorax 1999; 54:805-812

63. Nagaraju CK, Robinson EL, Abdesselem M, Trenson S, Dries E, Gilbert G, Janssens S, Van Cleemput J, Rega F, Meyns B, Roderick HL, Driesen RB, Sipido KR. Myofibroblast Phenotype and Reversibility of Fibrosis in Patients With End-Stage Heart Failure. J Am Coll Cardiol 2019; 73:2267-2282

64. Hara A, Kobayashi H, Asai N, Saito S, Higuchi T, Kato K, Okumura T, Bando YK, Takefuji M, Mizutani Y, Miyai Y, Saito S, Maruyama S, Maeda K, Ouchi N, Nagasaka A, Miyata T, Mii S, Kioka N, Worthley DL, Murohara T, Takahashi M, Enomoto A. Roles of the Mesenchymal Stromal/Stem Cell Marker Meflin in Cardiac Tissue Repair and the Development of Diastolic Dysfunction. Circ Res 2019; 125:414-430

65. Mizutani Y, Kobayashi H, Iida T, Asai N, Masamune A, Hara A, Esaki N, Ushida K, Mii S, Shiraki Y, Ando K, Weng L, Ishihara S, Ponik SM, Conklin MW, Haga H, Nagasaka A, Miyata T, Matsuyama M, Kobayashi T, Fujii T, Yamada S, Yamaguchi J, Wang T, Woods SL, Worthley D, Shimamura T, Fujishiro M, Hirooka Y, Enomoto A, Takahashi M. Meflin-Positive Cancer-Associated Fibroblasts Inhibit Pancreatic Carcinogenesis. Cancer Res 2019; 79:5367-5381

66. Li H, Zhao X, Shan H, Liang H. MicroRNAs in idiopathic pulmonary fibrosis: involvement in pathogenesis and potential use in diagnosis and therapeutics. Acta Pharm Sin B 2016; 6:531-539

67. Dennler S, Huet S, Gauthier JM. A short amino-acid sequence in MH1 domain is responsible for functional differences between Smad2 and Smad3. Oncogene 1999; 18:1643-1648

1180 **68.** Gu L, Zhu YJ, Yang X, Guo ZJ, Xu WB, Tian XL. Effect of TGF-beta/Smad
1181 signaling pathway on lung myofibroblast differentiation. Acta Pharmacol Sin
1182 2007; 28:382-391
1183 **69.** Micallef L, Vedrenne N, Billet F, Coulomb B, Darby IA, Desmouliere A. The
1184 myofibroblast, multiple origins for major roles in normal and pathological tissue
1185 repair. Fibrogenesis Tissue Repair 2012; 5:S5
1186 **70.** Desmouliere A, Geinoz A, Gabbiani F, Gabbiani G. Transforming growth factor-
1187 beta 1 induces alpha-smooth muscle actin expression in granulation tissue
1188 myofibroblasts and in quiescent and growing cultured fibroblasts. J Cell Biol
1189 1993; 122:103-111
1190 **71.** Driesen RB, Nagaraju CK, Abi-Char J, Coenen T, Lijnen PJ, Fagard RH, Sipido
1191 KR, Petrov VV. Reversible and irreversible differentiation of cardiac fibroblasts.
1192 Cardiovasc Res 2014; 101:411-422
1193 **72.** Noetel A, Kwiecinski M, Elfimova N, Huang J, Odenthal M. microRNA are
1194 Central Players in Anti- and Profibrotic Gene Regulation during Liver Fibrosis.
1195 Front Physiol 2012; 3:49
1196 **73.** Loboda A, Sobczak M, Jozkowicz A, Dulak J. TGF-beta1/Smads and miR-21 in
1197 Renal Fibrosis and Inflammation. Mediators Inflamm 2016; 2016:8319283
1198 **74.** Thum T, Gross C, Fiedler J, Fischer T, Kissler S, Bussen M, Galuppo P, Just S,
1199 Rottbauer W, Frantz S, Castoldi M, Soutschek J, Koteliansky V, Rosenwald A,
1200 Basson MA, Licht JD, Pena JT, Rouhanifard SH, Muckenthaler MU, Tuschl T,
1201 Martin GR, Bauersachs J, Engelhardt S. MicroRNA-21 contributes to myocardial
1202 disease by stimulating MAP kinase signalling in fibroblasts. Nature 2008;
1203 456:980-984
1204 **75.** Liu G, Friggeri A, Yang Y, Milosevic J, Ding Q, Thannickal VJ, Kaminski N,
1205 Abraham E. miR-21 mediates fibrogenic activation of pulmonary fibroblasts and
1206 lung fibrosis. J Exp Med 2010; 207:1589-1597
1207 **76.** Han M, Wang F, Gu Y, Pei X, Guo G, Yu C, Li L, Zhu M, Xiong Y, Wang Y.
1208 MicroRNA-21 induces breast cancer cell invasion and migration by suppressing
1209 smad7 via EGF and TGF-beta pathways. Oncol Rep 2016; 35:73-80
1210 **77.** Lehmann M, Buhl L, Alsafadi HN, Klee S, Hermann S, Mutze K, Ota C, Lindner
1211 M, Behr J, Hilgendorff A, Wagner DE, Konigshoff M. Differential effects of

1212 Nintedanib and Pirfenidone on lung alveolar epithelial cell function in ex vivo
1213 murine and human lung tissue cultures of pulmonary fibrosis. Respir Res 2018;
1214 19:175
1215

Supplementary Figure Legends

Supplementary Figure 1

Gating strategy used with lungs from bleomycin-administered AM+/- and WT mice.

Supplementary Figure 2

Time course of the lung weight and gene expression in bleomycin-induced pulmonary fibrosis in C57BL/6J wild-type mice

A: Appearance of lungs from control and bleomycin (BLM)-administered C57BL/6J wild-type (WT) mice. **B:** Lung weight ratios. The mean of the control group was assigned a value of 1 (n=5-9). **C:** Lung weight / body weight (mg/g) ratios (n=5-9). **D:** Quantitative real-time PCR analysis of AM-related genes (n=5). **E, F:** Quantitative real-time PCR analysis of inflammation-related genes (n=5). **G-J:** Quantitative real-time PCR analysis of fibrosis-related genes (n=5). In **D-J,** the means of the control groups were assigned a value of 1. Bars are means ± SEM. "*" indicates comparison between the groups. p-values were calculated using one-way ANOVA with Dunnett's test.

Supplementary Figure 3

Pathology of bleomycin-induced inflammation and fibrosis in the lungs of WT mice.

A: Representative photomicrographs of bleomycin-treated lung tissues from WT mice. Tissues were stained with hematoxylin / eosin (H&E) or Masson's trichrome (MT) or immunostained for α-smooth muscle actin (α-SMA), CD45, F4/80 or CD3. Scale bars in H&E and Masson's trichrome = 100 μm. Scale bars in α-SMA, CD45, F4/80 and CD3 immunostaining = 50 μm. **B:** Modified Ashcroft scores used to quantify pulmonary

fibrosis. **C:** Percentage of the Masson's trichrome stained fibrotic area / high-power field (HPF) (400x). **D:** Percentage of α-SMA-positive area / HPF (400x). **E-G:** Numbers of CD45-positive leukocytes (**E**), CD3-positive T cells (**F**) and F4/80-positve macrophages (**G**) / HPF (400x) (n=5-6). Bars are means ± SEM. "*" indicates comparison between the groups. p-values were calculated using one-way-ANOVA with Dunnett's test.

Supplementary Figure 4

Kaplan-Meier curves of bleomycin-administered AM+/- and WT mice (n=14).

Supplementary Figure 5

Bleomycin-induced pulmonary fibrosis is more severe in RAMP2+/- mice

A: Appearance of representative lungs from control and RAMP2+/- and WT mice on Day14 after bleomycin administration. **B:** Lung weight ratios. The mean of the WT control group was assigned a value of 1 (n=5-9). **C:** Lung weight / body weight (mg/g) ratios (n=5-9). **D:** Hydroxyproline levels in the lungs (n=4-8). **E, F:** Quantitative real-time PCR analysis of inflammation-related genes (n=5-7). **G-J:** Quantitative real-time PCR analysis of fibrosis-related genes (n=5-8). In **E-J,** the means of the WT control groups were assigned a value of 1. Bars are means ± SEM. "*" indicates comparison between the groups, "#" indicates comparison with WT control, "†" indicates comparison with RAMP2+/- control. p-values were calculated using two-way ANOVA with Tukey's test.

Supplementary Figure 6

Pathology of bleomycin-induced inflammation and fibrosis in the lungs of

RAMP2+/- mice

A, B: Representative photomicrographs of lung tissues stained with hematoxylin / eosin (H&E) or Masson's trichrome (MT) or immunostained for α-smooth muscle actin (α-SMA) on day 14 after bleomycin administration (**A**) and immunostaining for CD45, F4/80 or CD3 on day 7 after bleomycin administration (**B**). **Left column:** WT lungs, **Right column**: RAMP2+/- lungs. Scale bars for H&E and MT staining= 100 μm. Scale bars for α-SMA, CD45, F4/80 and CD3 immunostaining = 50 μm. **C:** Modified Ashcroft scores quantifying pulmonary fibrosis (n=5). **D:** Percentage of the Masson's trichrome-stained fibrotic area / HPF (400x) (n=5). **E:** Percentage of α-SMA positive area / HPF (400x) (n=5). **F-H:** Numbers of CD45-positve leukocytes (**F**), F4/80-positive macrophages (**G**) and CD3-positive T cells (**H)** / HPF (400x) (n=5). Bars are means ± SEM. "*" indicates comparison between the groups, "#" indicates comparison with WT control, "†" indicates comparison with RAMP2+/- control. p-values were calculated using two-way ANOVA with Tukey's test.

Supplementary Figure 7

AM-treatment ameliorates bleomycin-induced pulmonary fibrosis

A: Appearance of the lungs from control WT mice, bleomycin (BLM)-administered WT mice and BLM-administered WT mice treated with AM (Day 14). **B:** Lung weight ratios. The mean of the WT control group was assigned a value of 1 (n=5-11). **C:** Lung weight / body weight ratios (mg/g) (n=5-11). **D-F:** Quantitative real-time PCR analysis of inflammation-related (**D**, **E**) and fibrosis-related (**F**) genes in lungs left untreated (control) or bleomycin administration, with or without AM treatment (n=5-10). The means of the control groups were assigned a value of 1. Bars are means ± SEM. "#" indicates

comparison with WT control. "*" indicates comparison between the groups. p-values were calculated using one-way ANOVA with Dunnett's or Tukey's test.

Supplementary Figure 8

Pathology showing the effect of AM on bleomycin-induced inflammation and fibrosis in the lung

A: Representative photographs of lung tissues stained with hematoxylin/eosin (H&E) or Masson's trichrome (MT) or immunostained for α-smooth muscle actin (α-SMA) on day 14 after bleomycin treatment with and without AM (**A**) and immunostained for CD45, F4/80 or CD3 on day 7 after bleomycin treatment with and without AM (**B**). **Left column:** bleomycin-treated lungs, **Right column:** bleomycin-treated lungs with AM. Scale bars with H&E and MT staining = 100 μm. Scale bars in α-SMA, CD45, F4/80 and CD3 immunostaining = 50 μm. **C:** Modified Ashcroft scores quantifying pulmonary fibrosis (n=4-9). **D:** Percentage of the Masson's trichrome stained fibrotic area / HPF (400x) (n=4-9). **E:** Percentage of α-SMA positive area / HPF (400x) (n=4-9). **F-H:** Numbers of CD45-positve leukocytes (**F**), F4/80-positive macrophages (**G**) and CD3-positive T cells (**H)** / HPF (400x) (n=5). Bars are means ± SEM. "*" indicates comparison between the groups, "#" indicates comparison with control mice. p-values were calculated using one-way ANOVA with Tukey's test.

Supplementary Figure 9

Representative images of immunostained (Green: α-SMA, Red: Ki67, Blue: DAPI) lung sections from AM+/- and WT mice 14 days after bleomycin administration. Scale bars = 200 μm.

Table 1　Primers and probes used for real-time PCR

Adm (adrenomedullin)	Forward Reverse	5'-GGACACTGCAGGGCCAGAT-3' 5'-GTAGTTCCCTCTTCCCACGACTTA-3'
Ramp2 (RAMP2)	Probe Forward Reverse	5'-CCCAGAGGATGTGCTCCTGGCCAT-3' 5'-GCAGCCCACCTTCTCTGATC-3' 5'-AACGGGATGAGGCAGATGG-3'
Ramp3 (RAMP3)	Forward Reverse	5'-AAAGCCTTCGCTGACATGATG-3' 5'-ATCTCGGTGCAGTTAGTGAAGCT-3'
Calcrl (CLR)	Probe Forward Reverse	5'-ATCGTGGTGGCTGTGTTTGCGGAG-3' 5'-AGGCGTTTACCTGCACACACT-3' CAGGAAGCAGAGGAAACCCC-3'
Il-6 (IL-6)	Forward Reverse	5'-CTGCAAGAGACTTCCATCCAGTT-3' 5'-GAAGTAGGGAAGGCCGTGG-3'
Ccl2 (MCP-1)	Forward Reverse	5'-GCAGTTAACGCCCCACTCA-3' 5'-CCTACTCATTGGGATCATCTTGCT-3'
Col1a1 (Type I collagen α1)	Forward Reverse	5'-ATGGATTCCCGTTCGAGTACG-3' 5'-TCAGCTGGATAGCGACATCG-3'
Spp1 (Osteopontin)	Probe Forward Reverse	5'-CCCAGCTTCTGAGCATGCCCTCTG-3' 5'-CCCTCGATGTCATCCCTGTT-3' 5'-CCCTTTCCGTTGTTGTCCTG-3'
Fn1 (Fibronectin)	Forward Reverse	5'-GGCTACATCATCCGCCATCA-3' 5'-GCCCGGATTAAGGTTGGTGA-3'
Acta2 (α-SMA)	Forward Reverse	5'-CCACCGCAAATGCTTCTAAGT-3' 5'-GGCAGGAATGATTTGGAAAGG-3'
Tgfb1 (TGF-β1)	Forward Reverse	5'-CCCGAAGCGGACTACTATGC-3' 5'-TAGATGGCGTTGTTGCGGT-3'
Timp1 (TIMP-1)	Forward Reverse	5'-CCGCCTAAGGAACGGAAATT-3' 5'-GGGCTCAGAGTACGCCAGG-3'
Islr (Meflin)	Forward Reverse	5'-AGATCCGCTCGGTGGCTATT-3' 5'-AGGTCGCTCCAGGCAAACT-3'

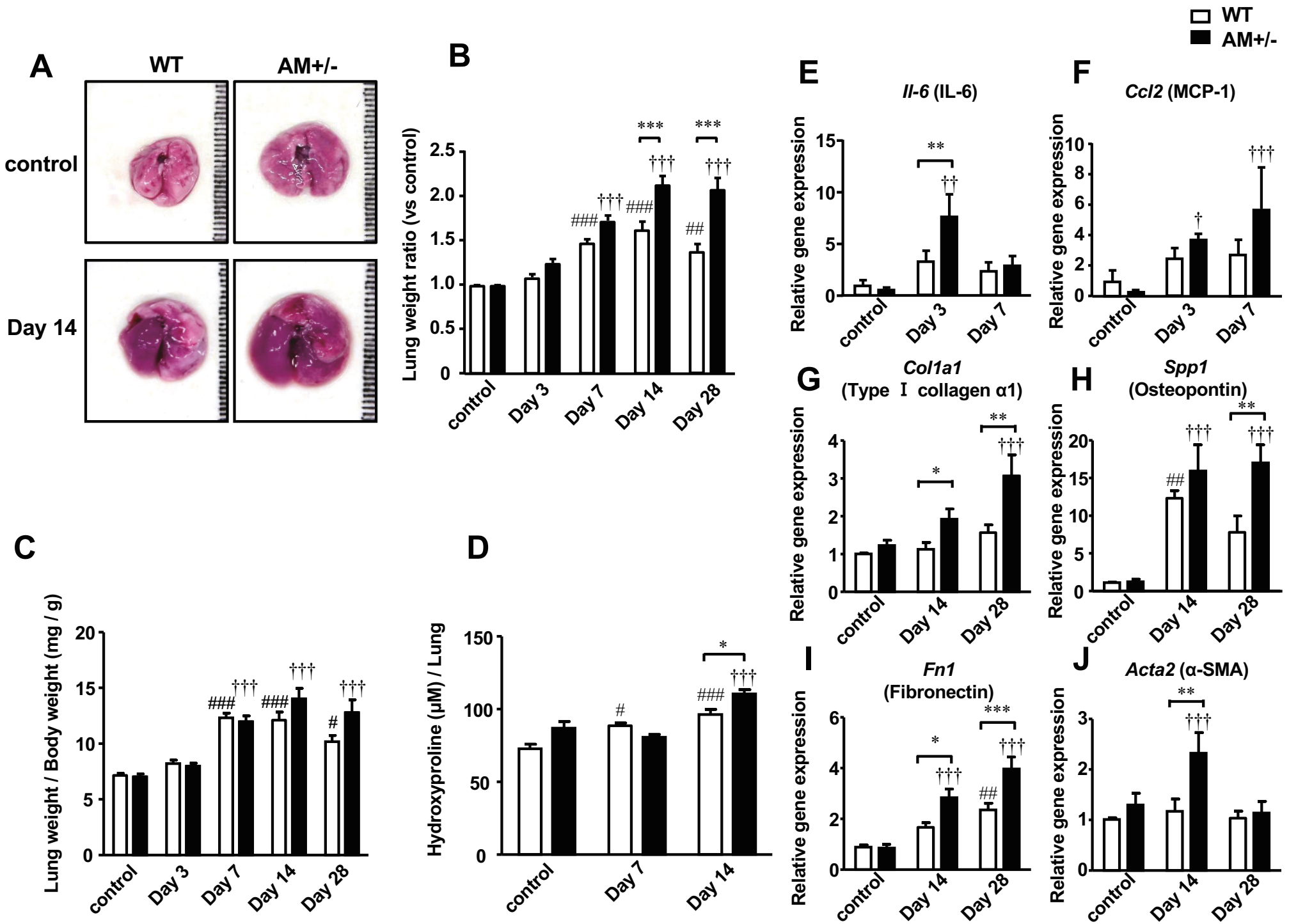

Figure 1

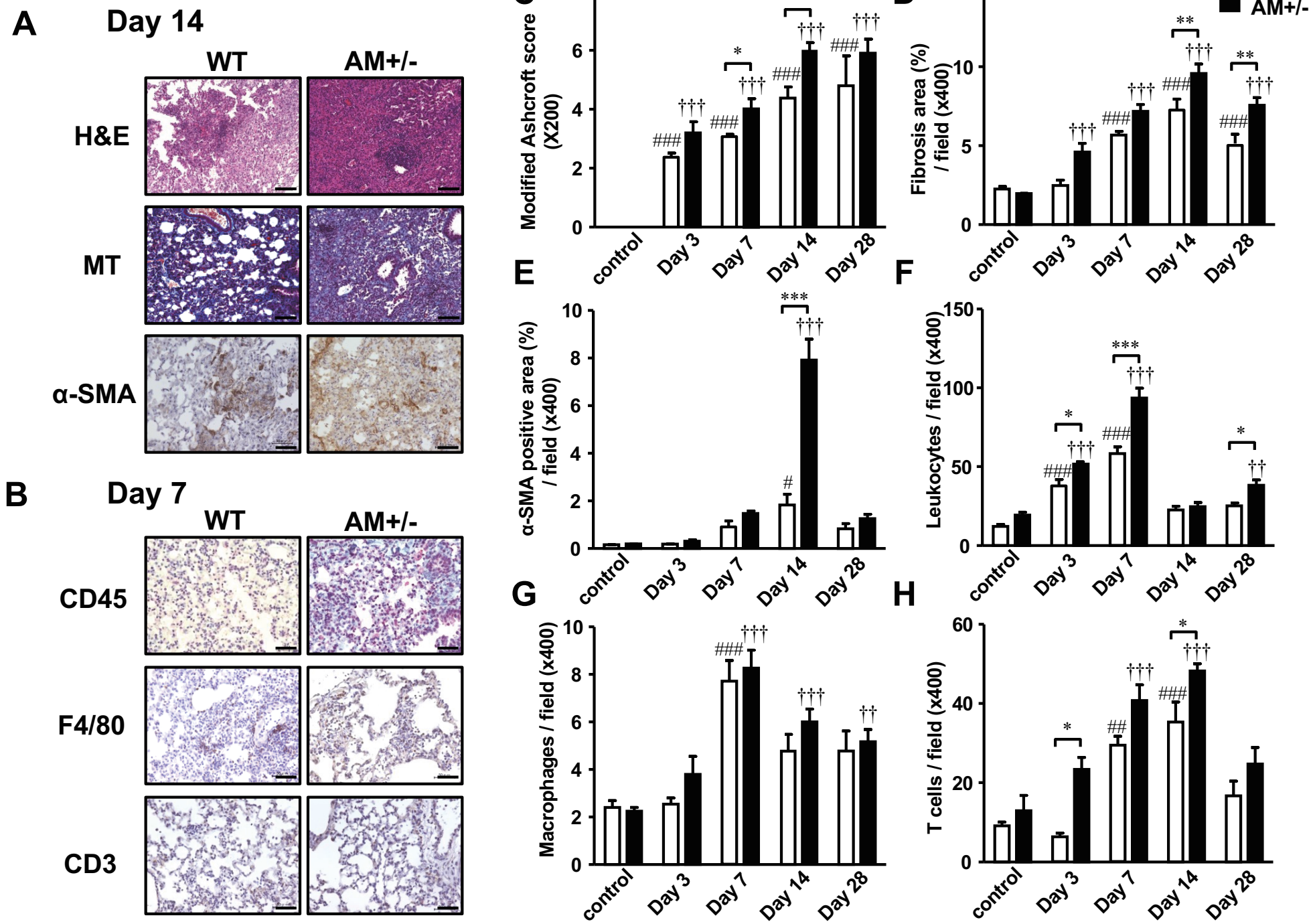
A
Day 14
WT
AM+/-
H&E
MT
α-SMA
B
Day 7
WT
AM+/-
CD45
F4/80
CD3
C
Modified Ashcroft score (X200)
D
Fibrosis area (%) / field (x400)
WT
AM+/-
E
α-SMA positive area (%) / field (x400)
F
Leukocytes / field (x400)
G
Macrophages / field (x400)
H
T cells / field (x400)
control
Day 3
Day 7
Day 14
Day 28

Figure 2

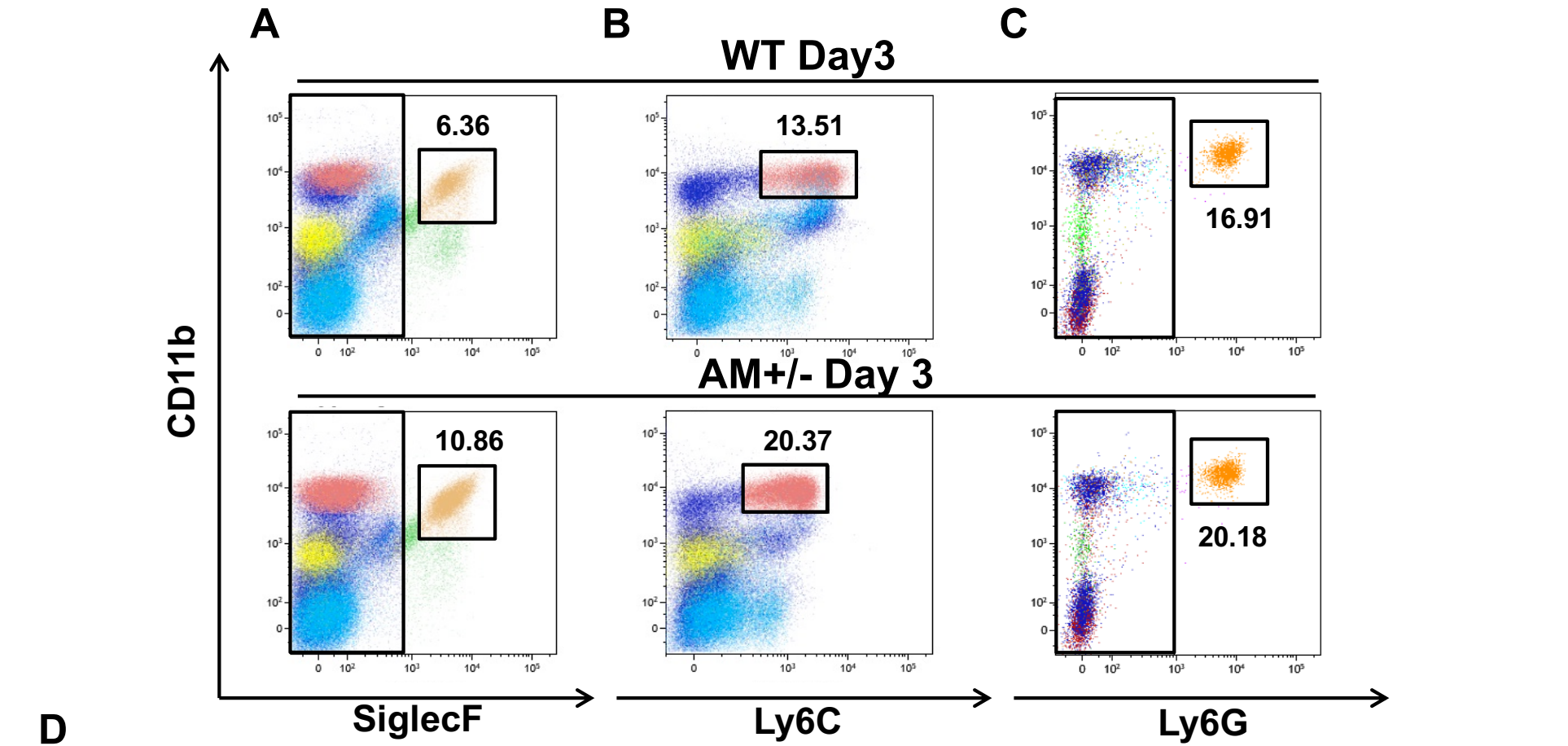
A
B
C
WT Day3
6.36
13.51
16.91
AM+/- Day 3
10.86
20.37
20.18
CD11b
SiglecF
Ly6C
Ly6G

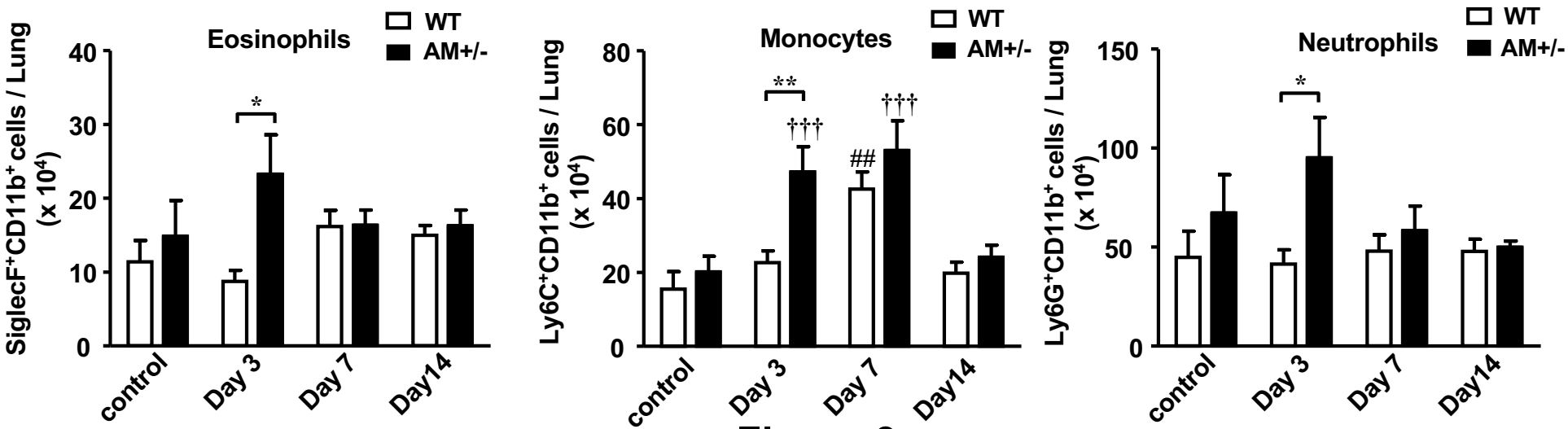
D
Eosinophils
WT
AM+/-
SiglecF+CD11b+ cells / Lung (x 10^4)
control
Day 3
Day 7
Day14
Monocytes
Ly6C+CD11b+ cells / Lung (x 10^4)
Neutrophils
Ly6G+CD11b+ cells / Lung (x 10^4)

Figure 3

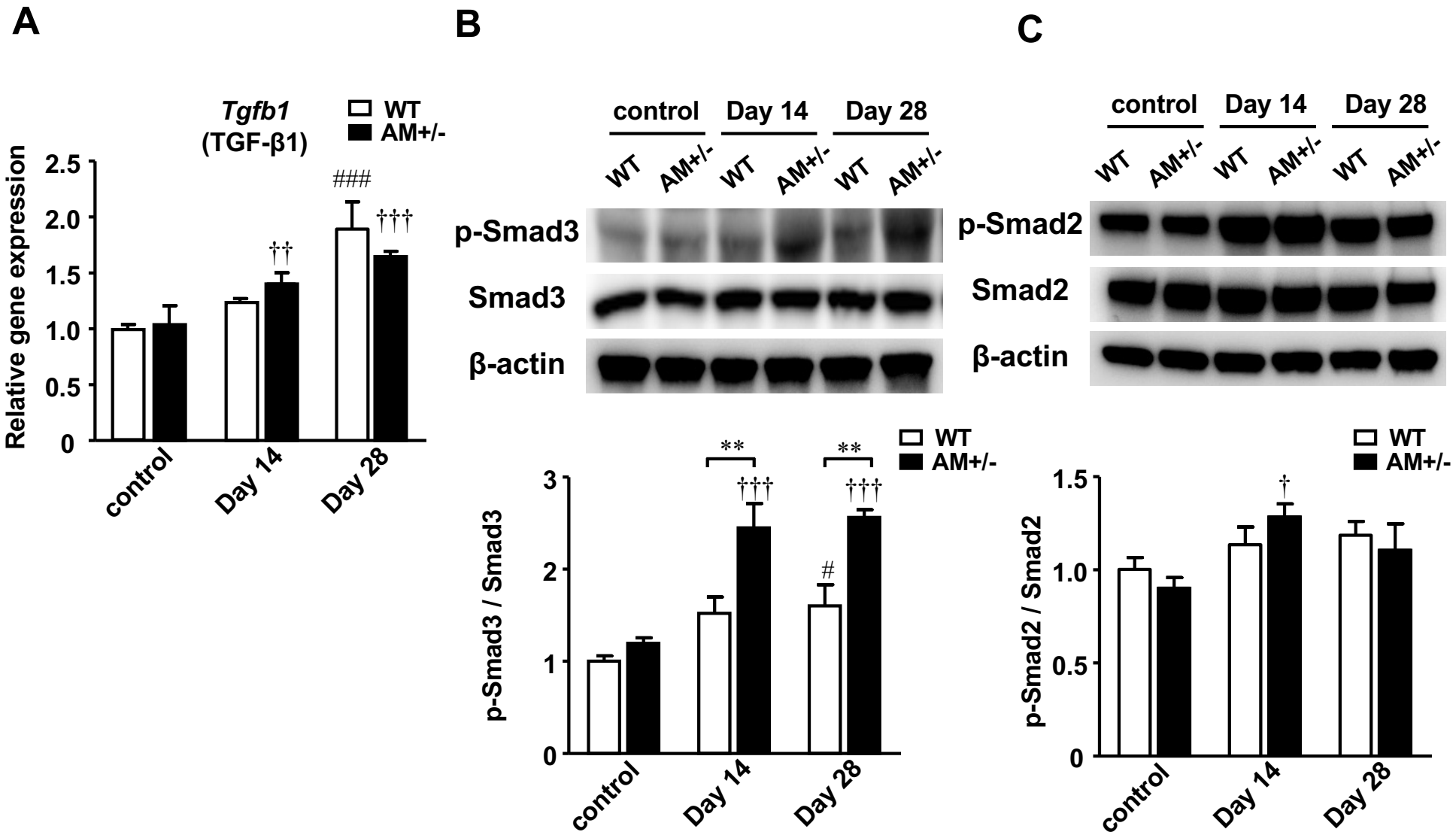
A
Tgfb1
(TGF-β1)
WT
AM+/-
Relative gene expression
2.5
2.0
1.5
1.0
0.5
0
###
††
†††
control
Day 14
Day 28
B
control
Day 14
Day 28
WT
AM+/-
p-Smad3
Smad3
β-actin
p-Smad3 / Smad3
**
**
†††
†††
#
C
p-Smad2
Smad2
β-actin
p-Smad2 / Smad2
†

Figure 4

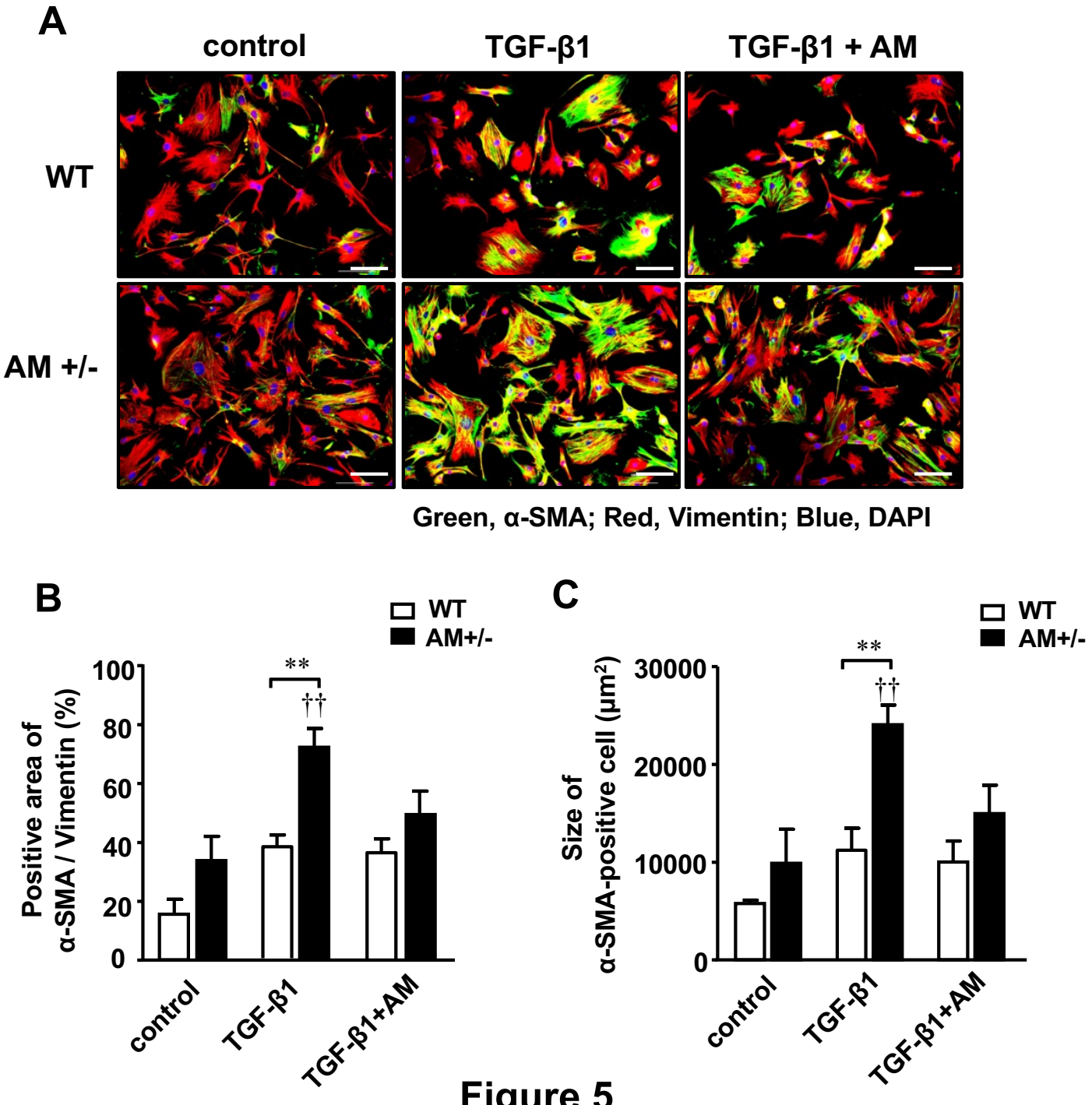
A
control
TGF-β1
TGF-β1 + AM
WT
AM +/-
Green, α-SMA; Red, Vimentin; Blue, DAPI
B
WT
AM+/-
Positive area of α-SMA / Vimentin (%)
100
80
60
40
20
0
**
††
control
TGF-β1
TGF-β1+AM
C
WT
AM+/-
Size of α-SMA-positive cell (μm²)
30000
20000
10000
0
**
††
control
TGF-β1
TGF-β1+AM

Figure 5

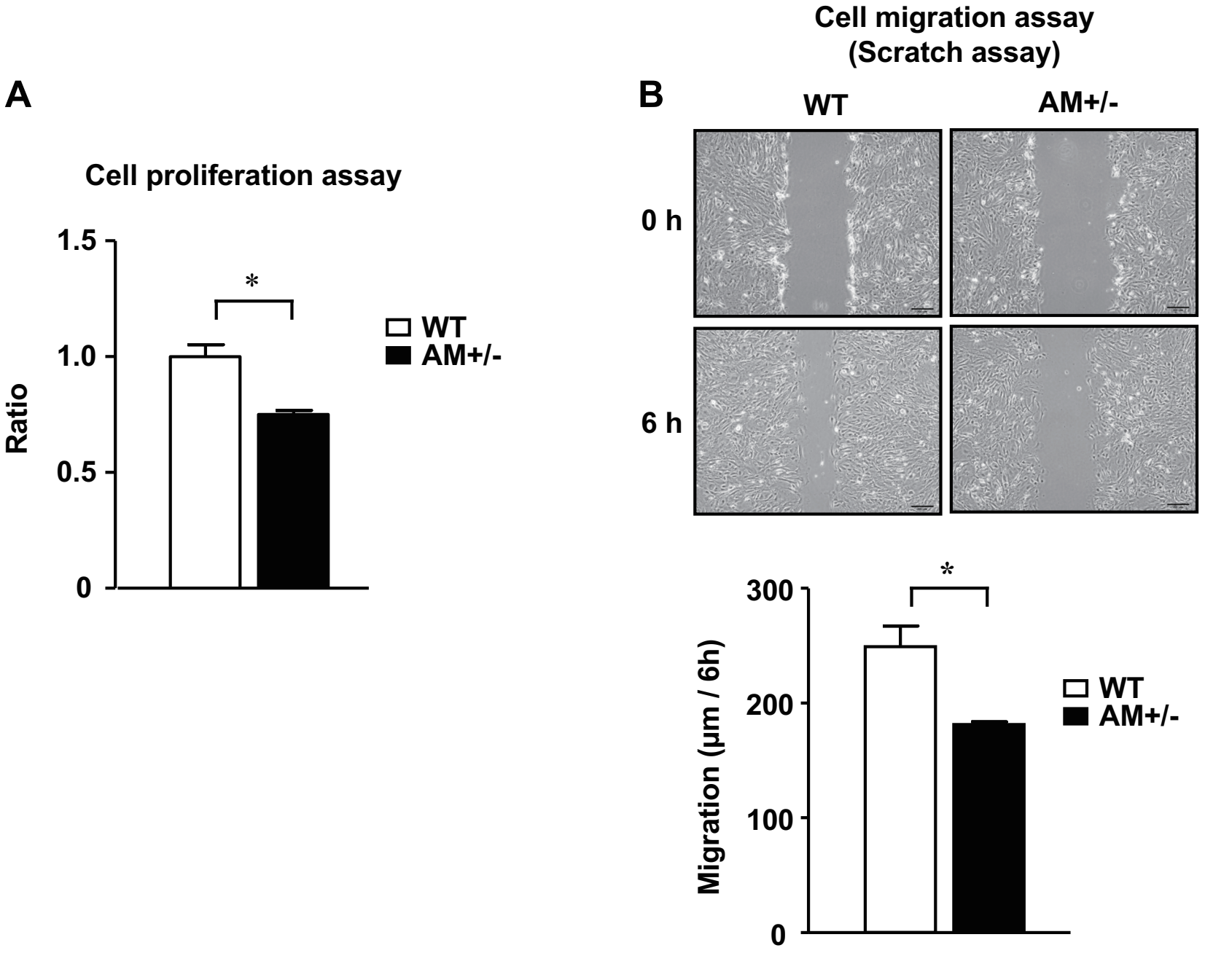
A
Cell proliferation assay
Ratio
1.5
1.0
0.5
0
*
WT
AM+/-
B
Cell migration assay
(Scratch assay)
WT
AM+/-
0 h
6 h
Migration (μm / 6h)
300
200
100
0
*
WT
AM+/-

Figure 6

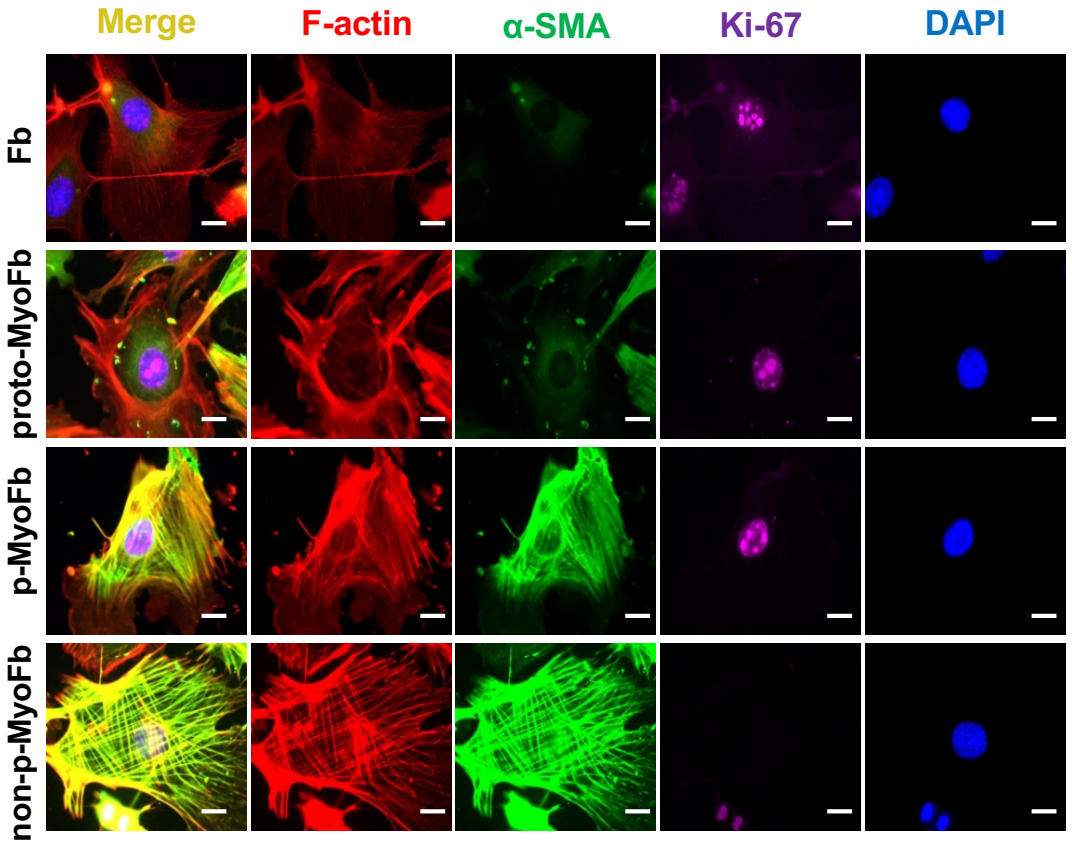

	F-actin	α-SMA	Ki-67
fibroblast (Fb)	+/−	−	+
proto-myofibroblast (proto-MyoFb)	+	−	+
proliferating-myofibroblast (p-MyoFb)	+	+	+
nonproliferating-myofibroblast (non-p-MyoFb)	+	+	−

Figure 7

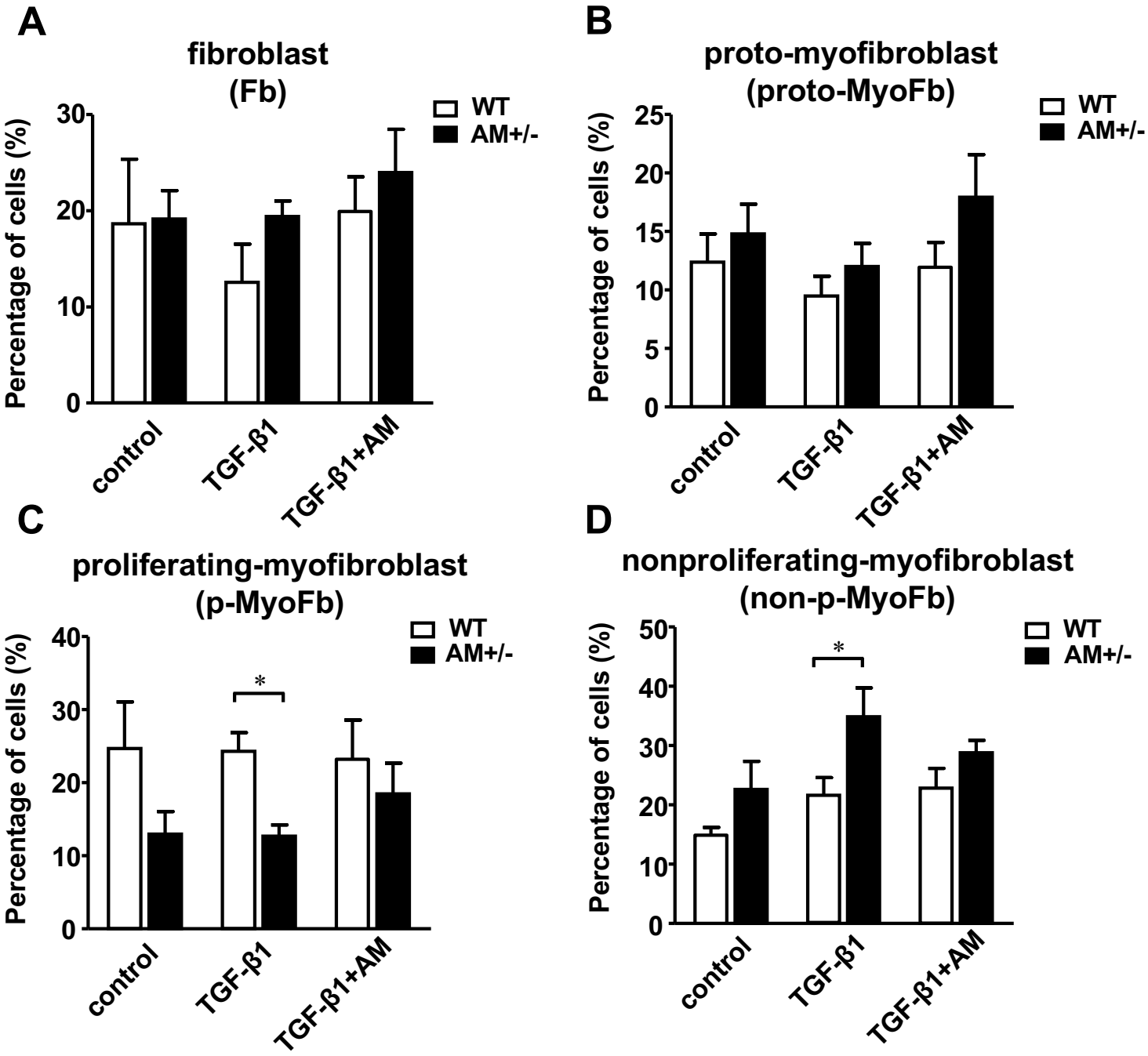
A
fibroblast
(Fb)
Percentage of cells (%)
30
20
10
0
WT
AM+/-
control
TGF-β1
TGF-β1+AM
B
proto-myofibroblast
(proto-MyoFb)
Percentage of cells (%)
25
20
15
10
5
0
WT
AM+/-
control
TGF-β1
TGF-β1+AM
C
proliferating-myofibroblast
(p-MyoFb)
Percentage of cells (%)
40
30
20
10
0
*
WT
AM+/-
control
TGF-β1
TGF-β1+AM
D
nonproliferating-myofibroblast
(non-p-MyoFb)
Percentage of cells (%)
50
40
30
20
10
0
*
WT
AM+/-
control
TGF-β1
TGF-β1+AM

Figure 8

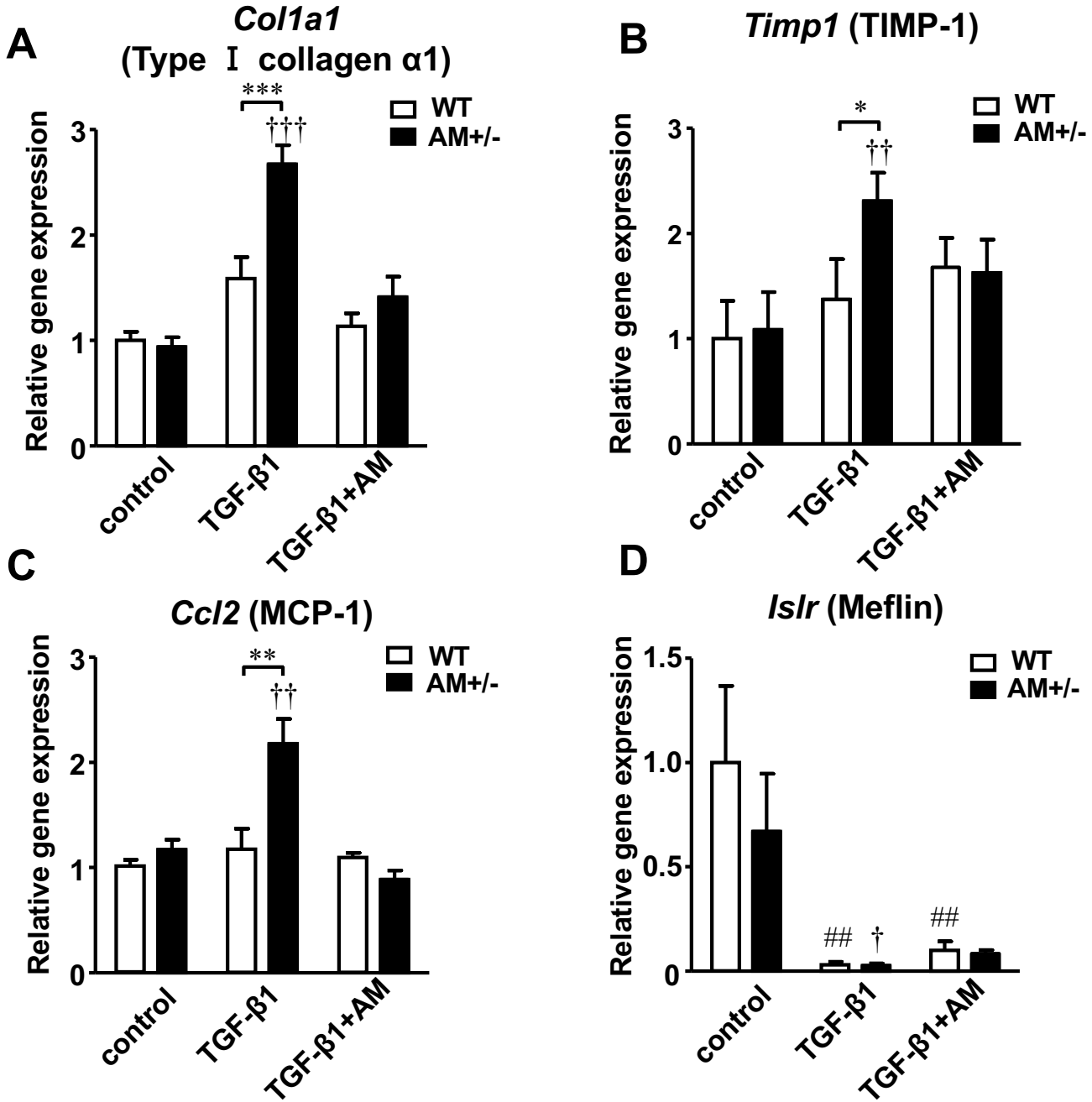
A
Col1a1
(Type Ⅰ collagen α1)
***
†††
WT
AM+/-
Relative gene expression
3
2
1
0
control
TGF-β1
TGF-β1+AM
B
Timp1 (TIMP-1)
*
††
WT
AM+/-
Relative gene expression
3
2
1
0
control
TGF-β1
TGF-β1+AM
C
Ccl2 (MCP-1)
**
††
WT
AM+/-
Relative gene expression
3
2
1
0
control
TGF-β1
TGF-β1+AM
D
Islr (Meflin)
WT
AM+/-
Relative gene expression
1.5
1.0
0.5
0
†
##
control
TGF-β1
TGF-β1+AM

Figure 9

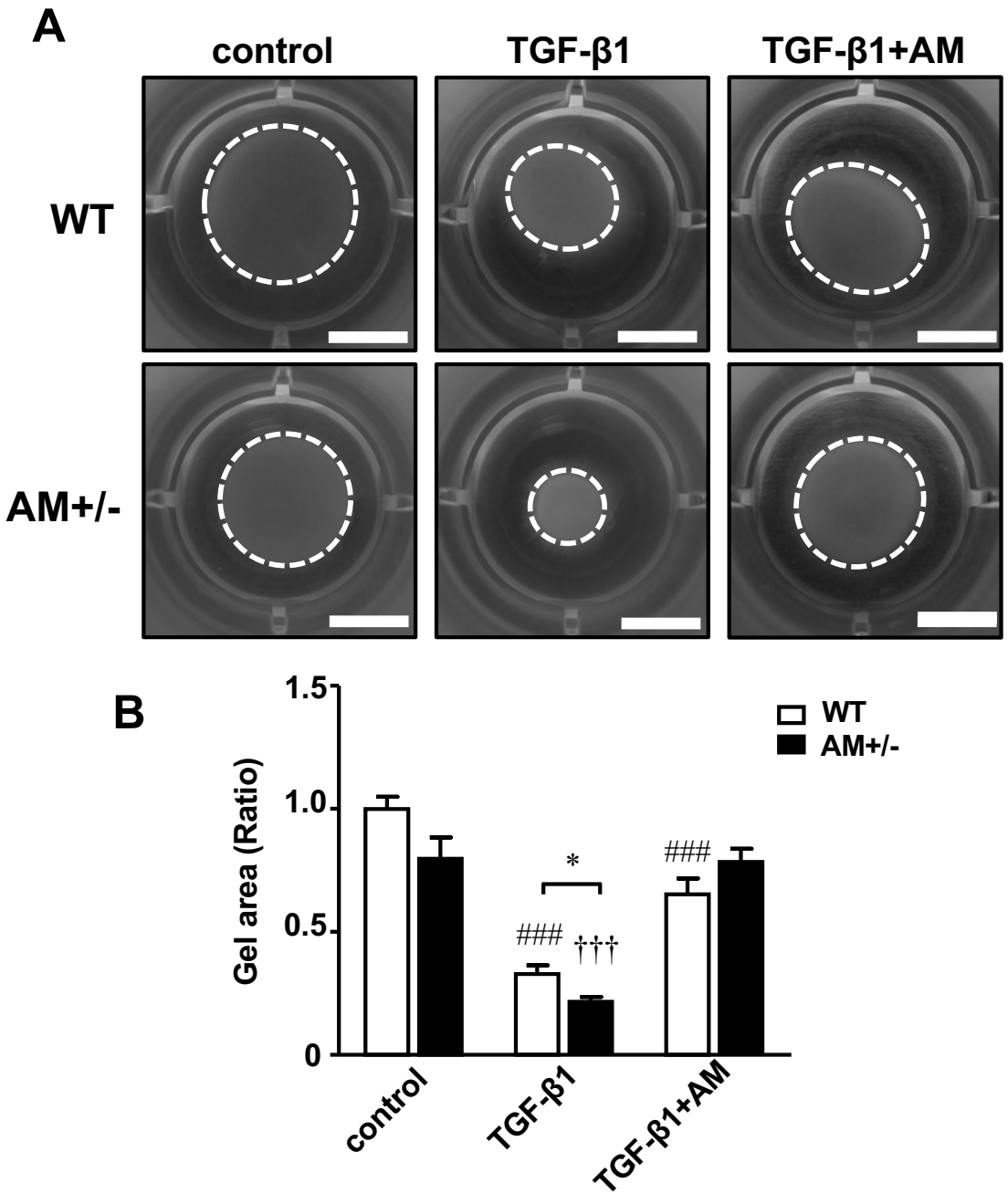
A
control
TGF-β1
TGF-β1+AM
WT
AM+/-
B
Gel area (Ratio)
1.5
1.0
0.5
0
WT
AM+/-
*
###
###
†††
control
TGF-β1
TGF-β1+AM

Figure 10

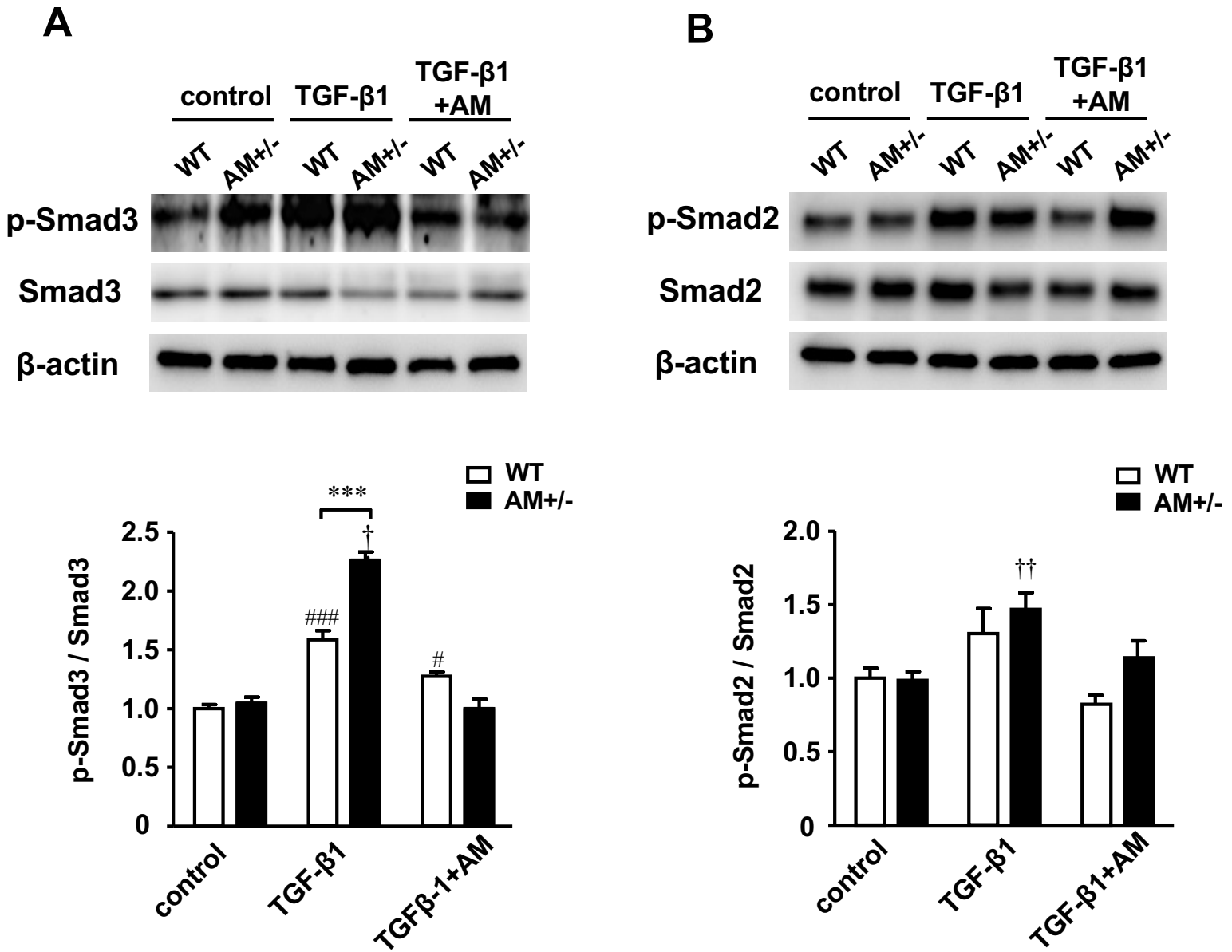
A
control
TGF-β1
TGF-β1 +AM
WT
AM+/-
p-Smad3
Smad3
β-actin
B
p-Smad2
Smad2
WT
AM+/-
p-Smad3 / Smad3
***
†
###
#
2.5
2.0
1.5
1.0
0.5
0
control
TGF-β1
TGFβ-1+AM
p-Smad2 / Smad2
††
TGF-β1+AM

Figure 11

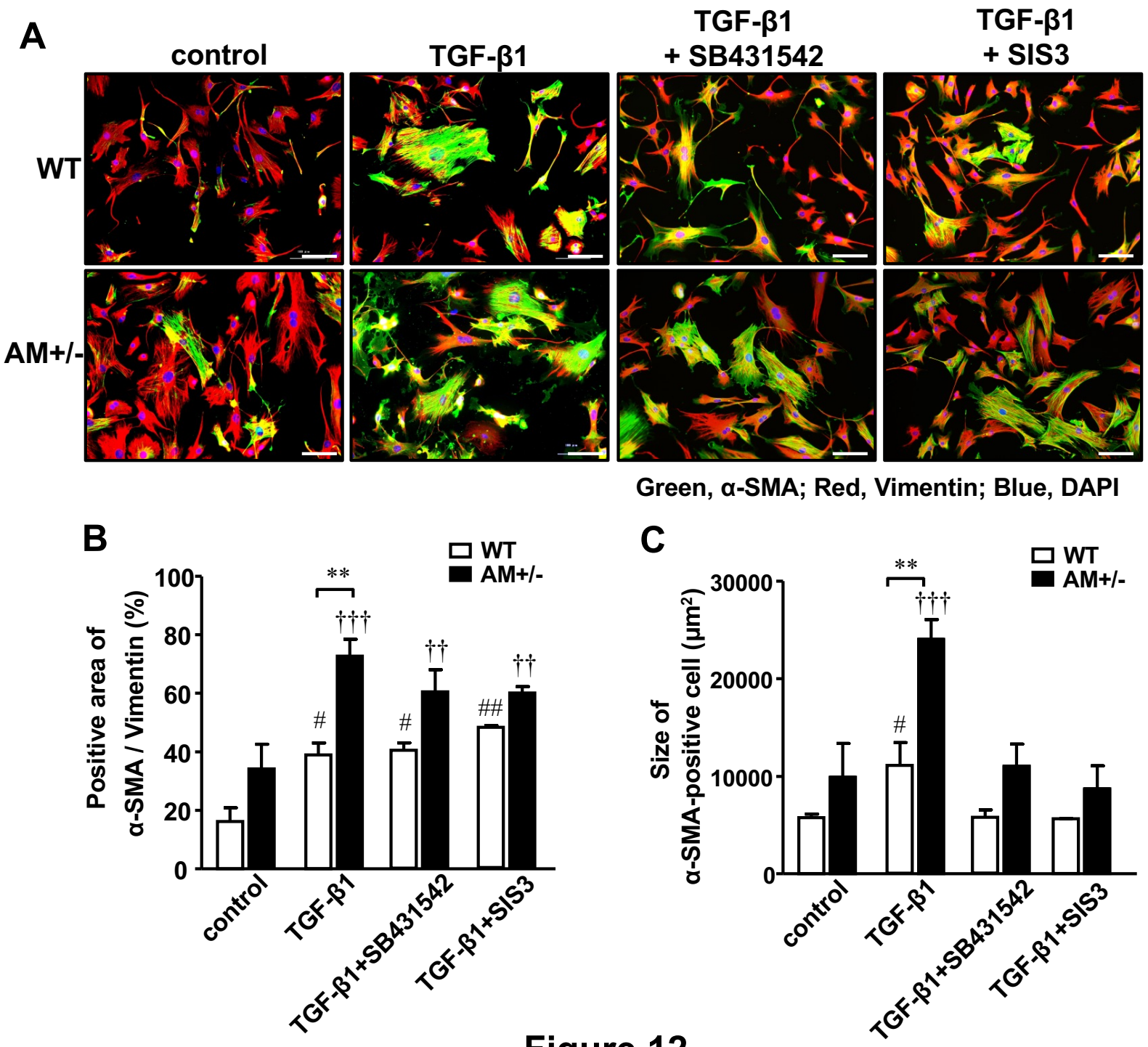
A
control
TGF-β1
TGF-β1
+ SB431542
TGF-β1
+ SIS3
WT
AM+/-
Green, α-SMA; Red, Vimentin; Blue, DAPI
B
WT
AM+/-
Positive area of
α-SMA / Vimentin (%)
100
80
60
40
20
0
**
†††
#
††
#
††
##
control
TGF-β1
TGF-β1+SB431542
TGF-β1+SIS3
C
WT
AM+/-
Size of
α-SMA-positive cell (μm²)
30000
20000
10000
0
**
†††
#
control
TGF-β1
TGF-β1+SB431542
TGF-β1+SIS3

Figure 12

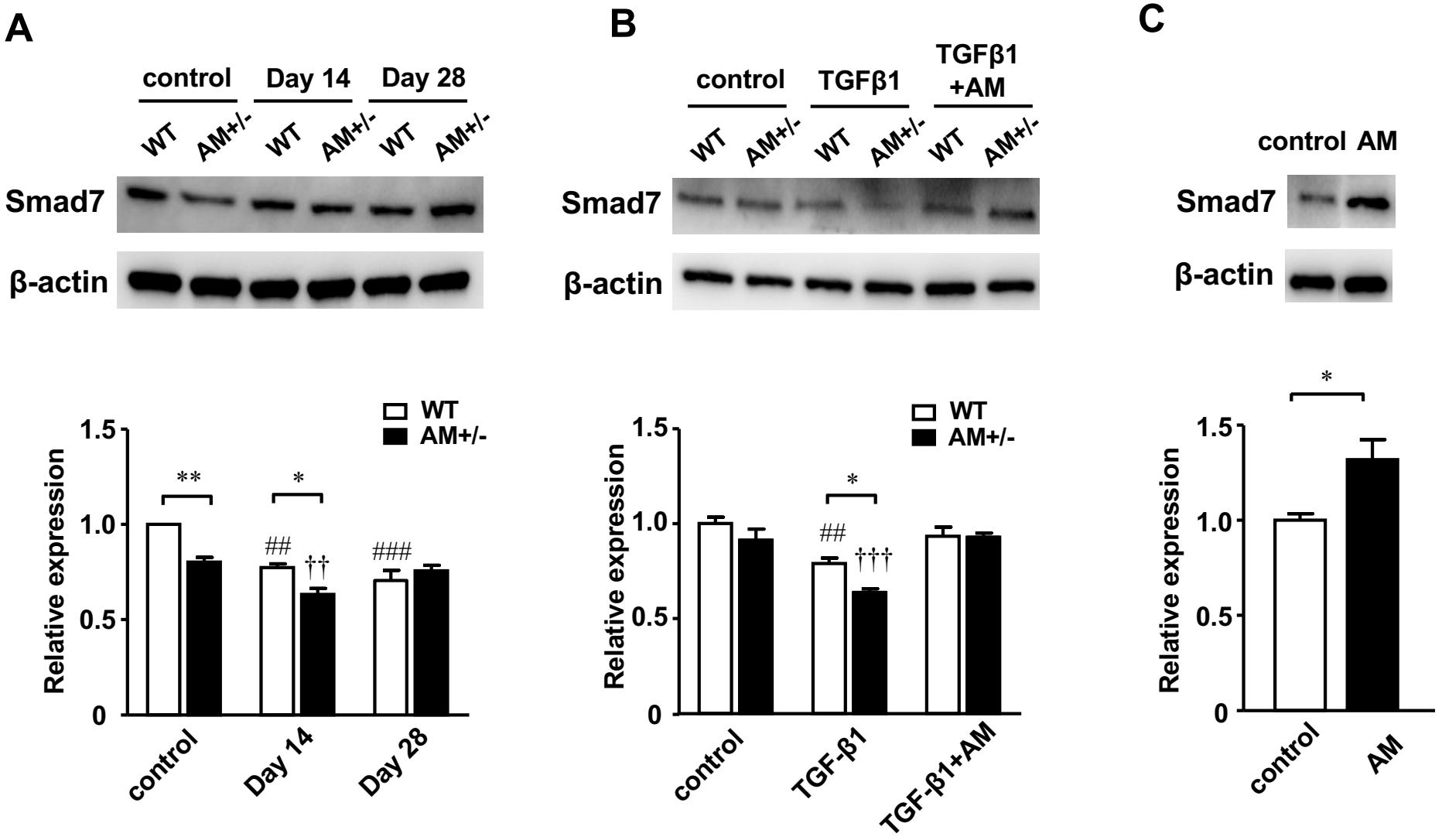
A
control
Day 14
Day 28
WT
AM+/-
Smad7
β-actin
Relative expression
WT
AM+/-
**
*
##
††
###
control
Day 14
Day 28
B
control
TGFβ1
TGFβ1 +AM
Smad7
β-actin
*
##
†††
control
TGF-β1
TGF-β1+AM
C
control
AM
Smad7
β-actin
*
control
AM

Figure 13

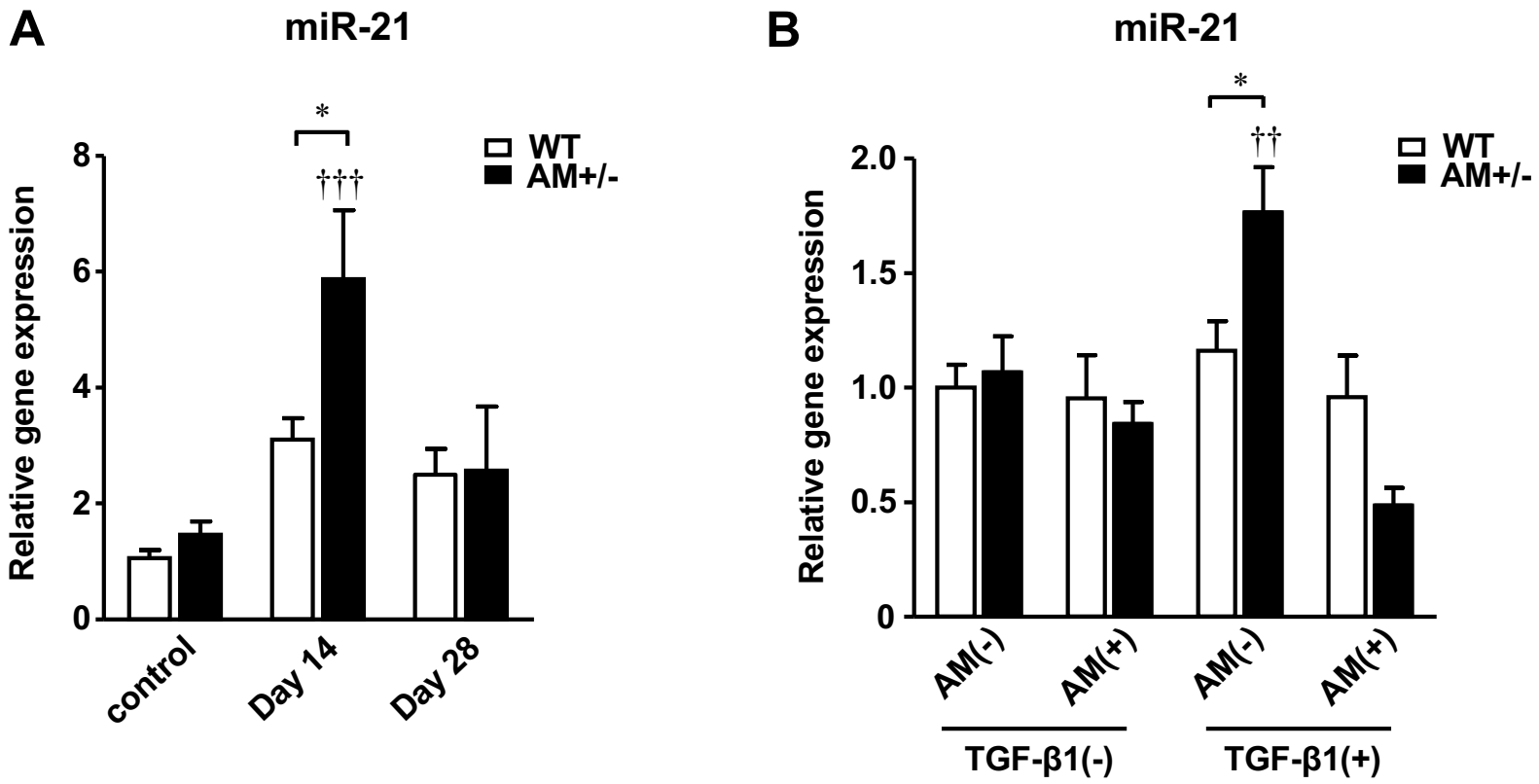
A
miR-21
Relative gene expression
8
6
4
2
0
*
†††
WT
AM+/-
control
Day 14
Day 28
B
miR-21
Relative gene expression
2.0
1.5
1.0
0.5
0
*
††
WT
AM+/-
AM(-)
AM(+)
AM(-)
AM(+)
TGF-β1(-)
TGF-β1(+)

Figure 14

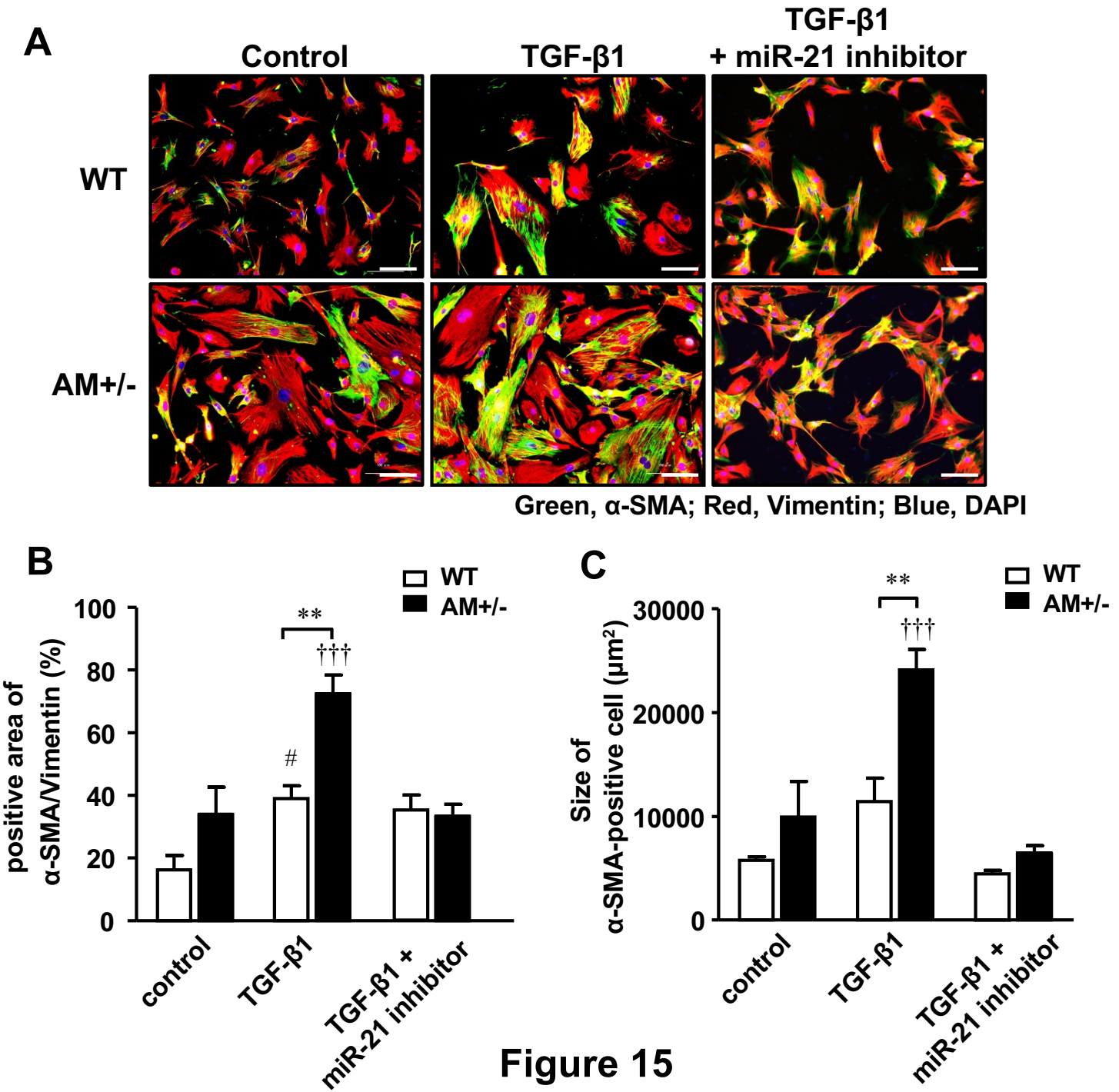
A
Control
TGF-β1
TGF-β1
+ miR-21 inhibitor
WT
AM+/-
Green, α-SMA; Red, Vimentin; Blue, DAPI
B
WT
AM+/-
positive area of
α-SMA/Vimentin (%)
100
80
60
40
20
0
**
†††
#
control
TGF-β1
TGF-β1 +
miR-21 inhibitor
C
WT
AM+/-
Size of
α-SMA-positive cell (μm²)
30000
20000
10000
0
**
†††
control
TGF-β1
TGF-β1 +
miR-21 inhibitor

Figure 15

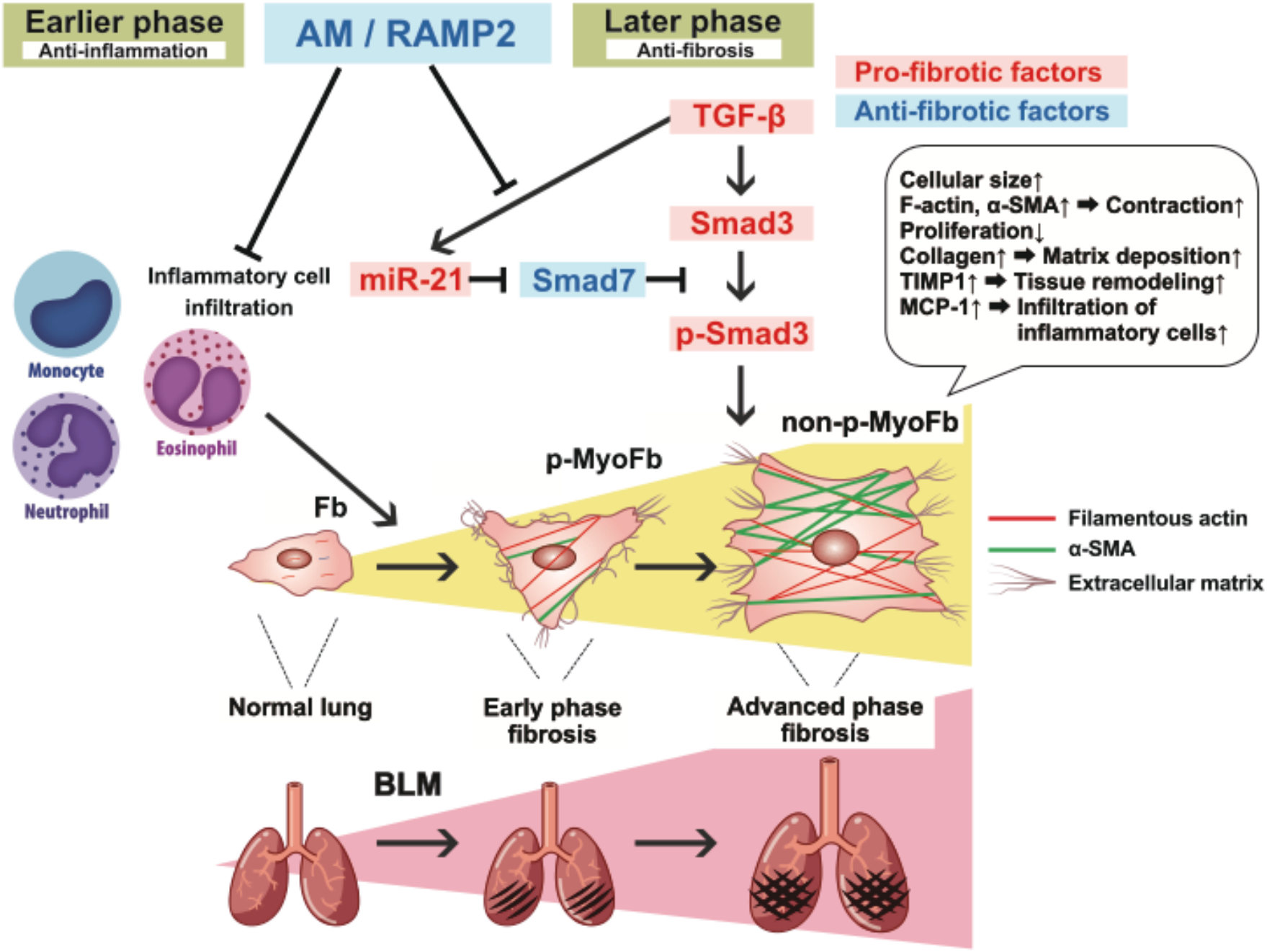
Earlier phase
Anti-inflammation
AM / RAMP2
Later phase
Anti-fibrosis
Pro-fibrotic factors
Anti-fibrotic factors
TGF-β
Smad3
Cellular size↑
F-actin, α-SMA↑ ➡ Contraction↑
Proliferation↓
Collagen↑ ➡ Matrix deposition↑
TIMP1↑ ➡ Tissue remodeling↑
MCP-1↑ ➡ Infiltration of inflammatory cells↑
Inflammatory cell infiltration
miR-21
Smad7
p-Smad3
Monocyte
Eosinophil
Neutrophil
non-p-MyoFb
p-MyoFb
Fb
Filamentous actin
α-SMA
Extracellular matrix
Normal lung
Early phase fibrosis
Advanced phase fibrosis
BLM

Figure 16

Supplementary Figure

Click here to access/download;Figure;210330Supplementary Figure.pdf

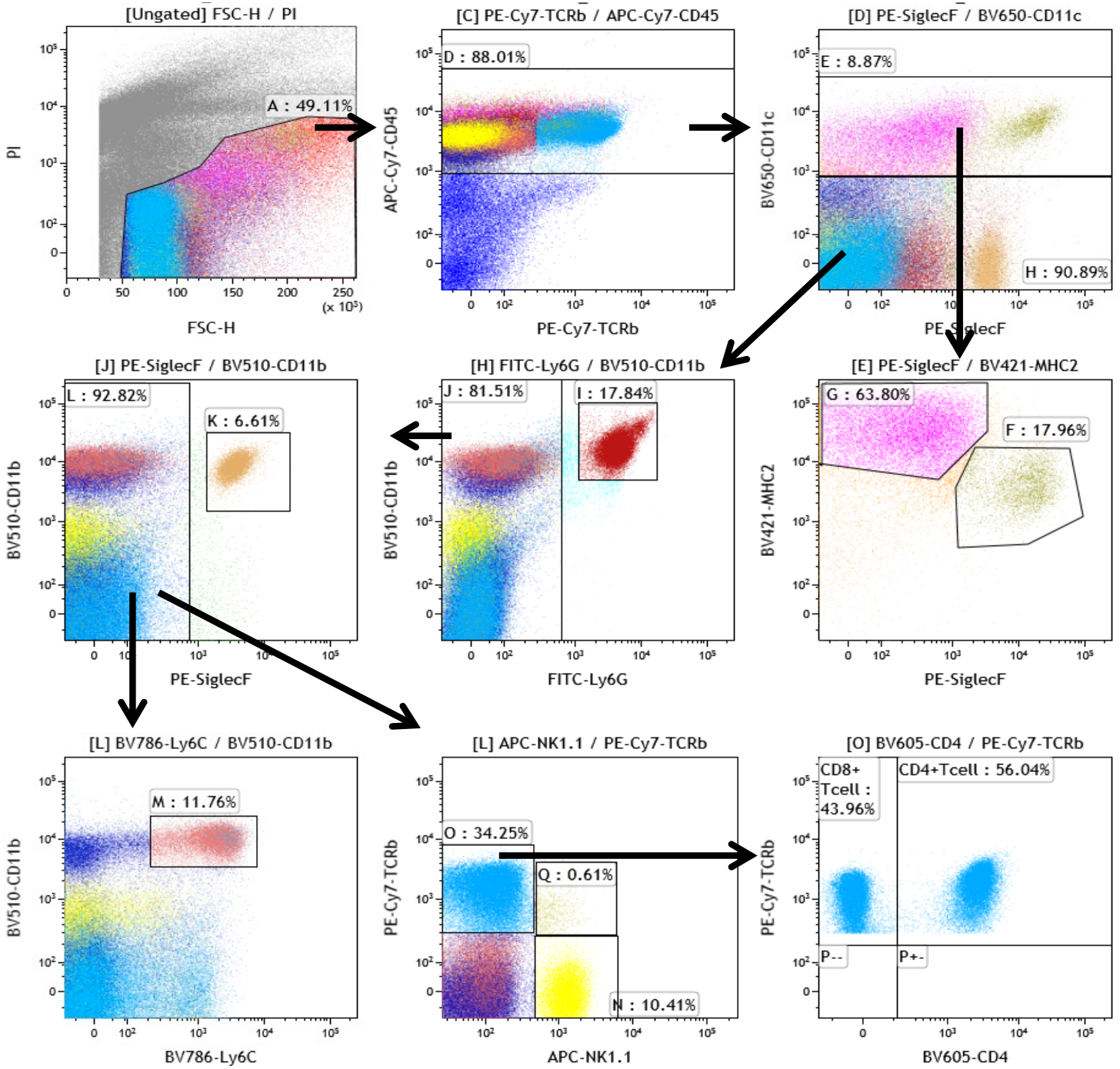

Supplementary Figure 1

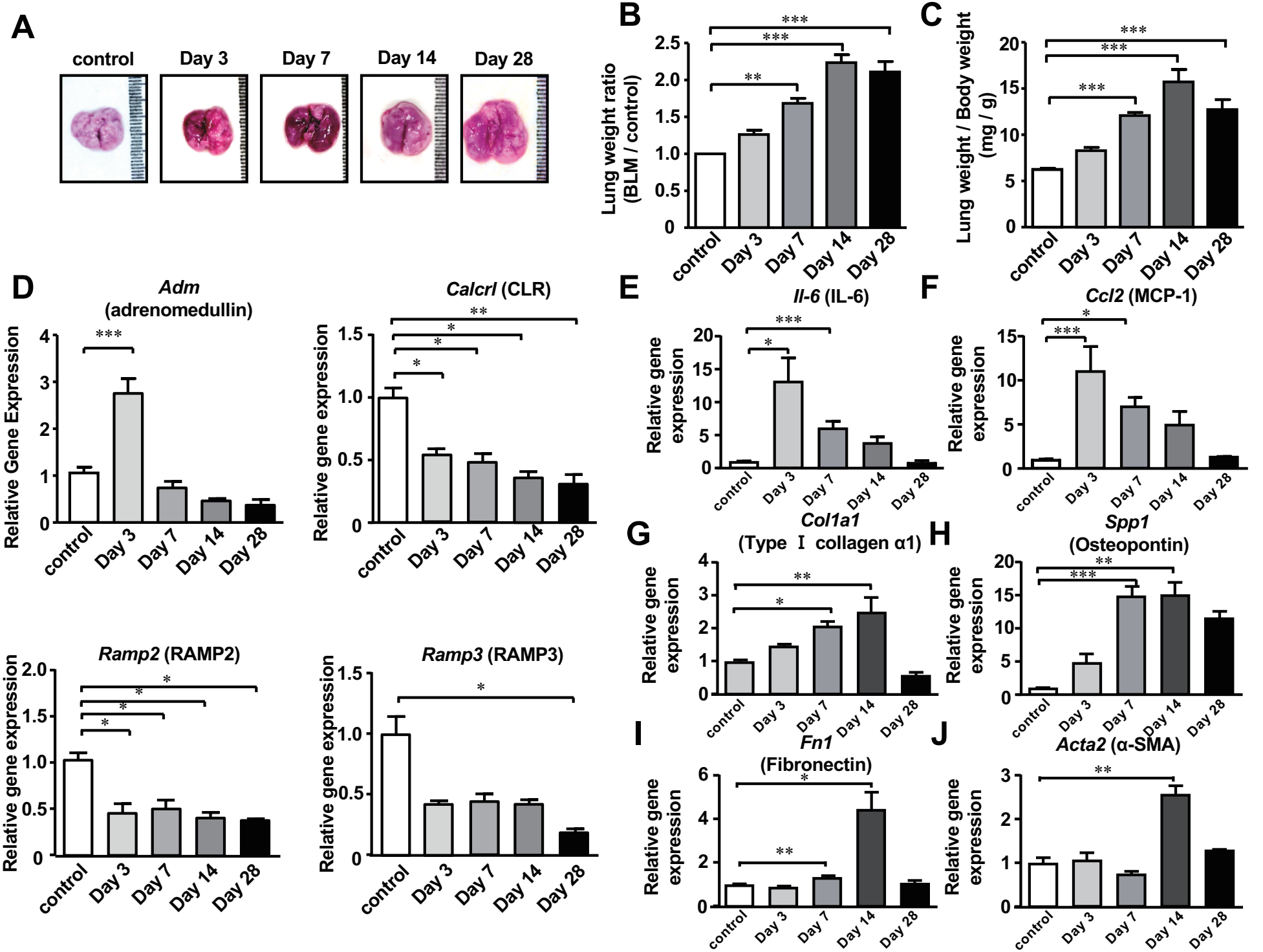

Supplementary Figure 2

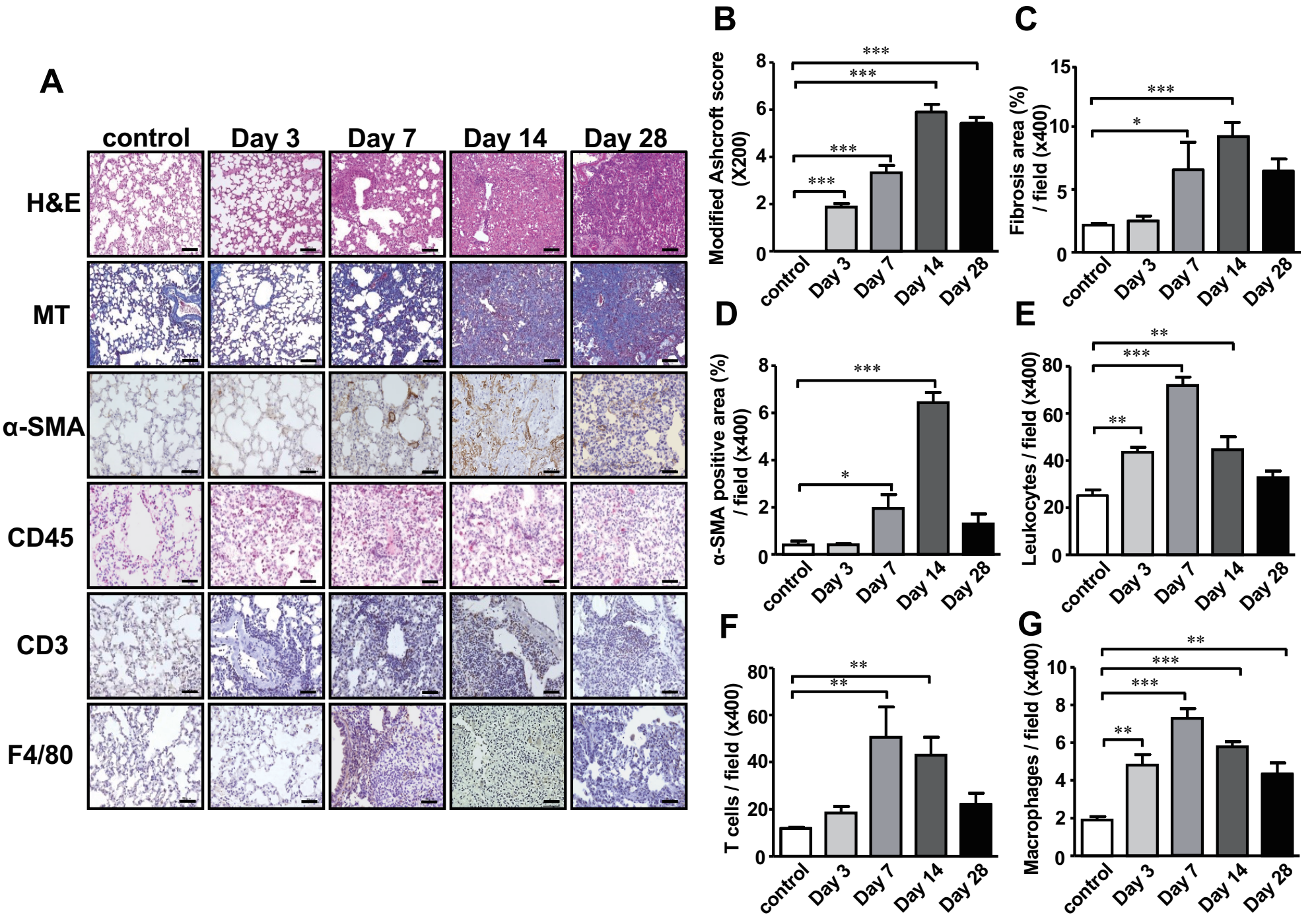

Supplementary Figure 3

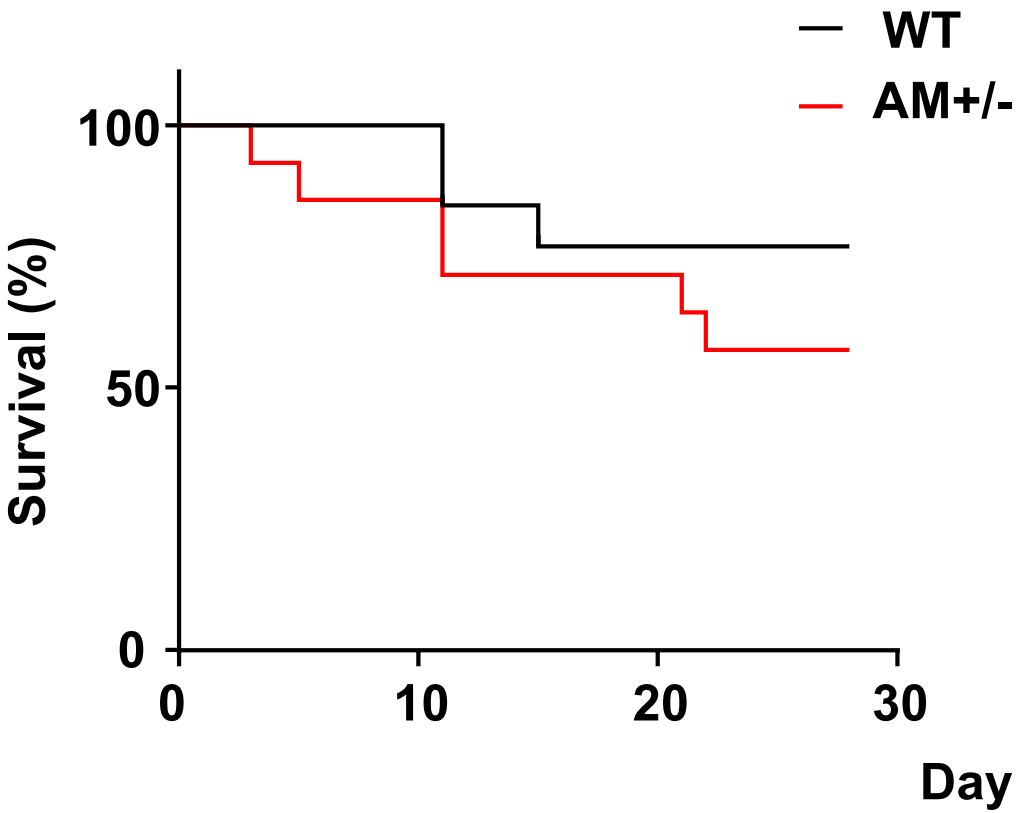

Supplementary Figure 4

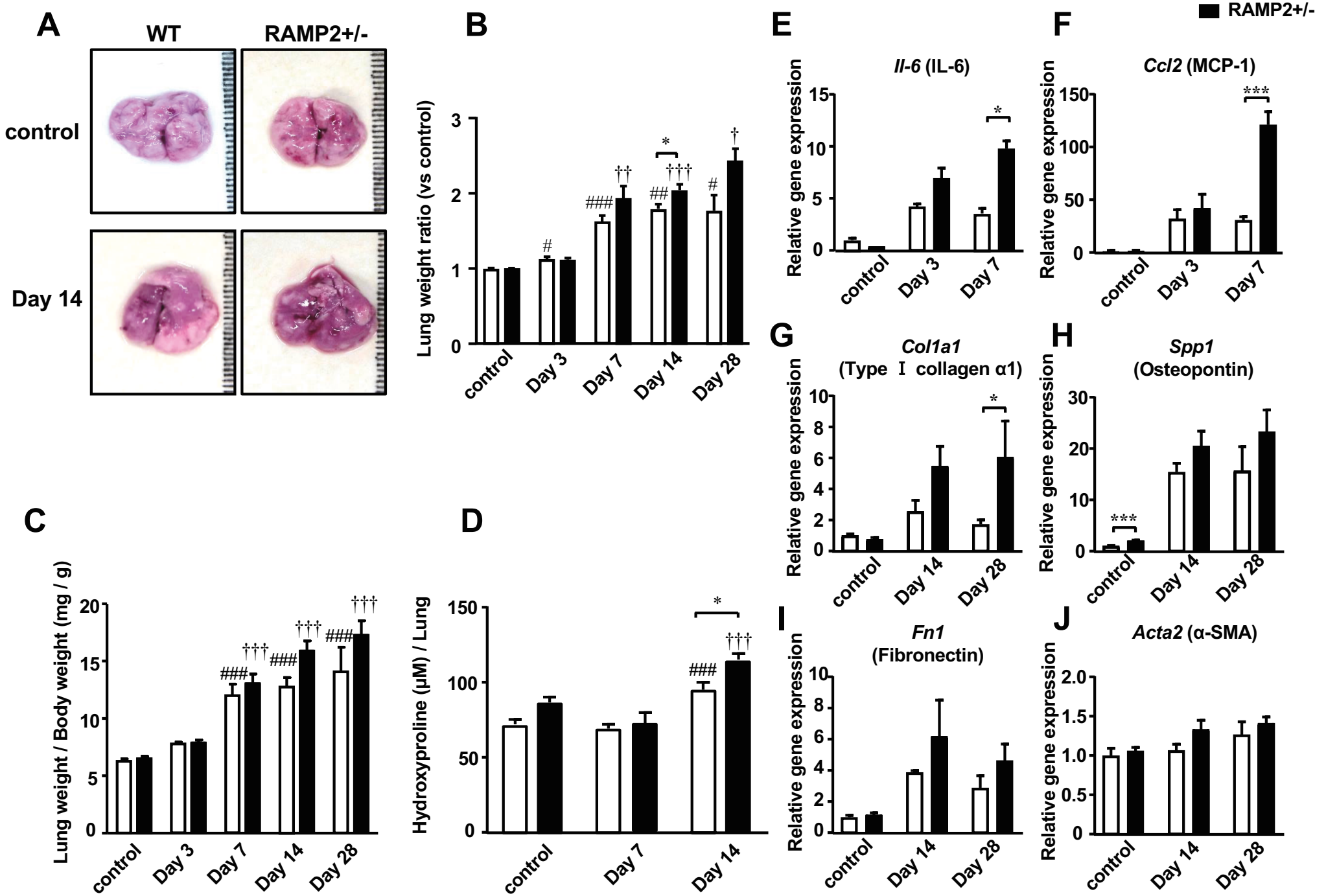

Supplementary Figure 5

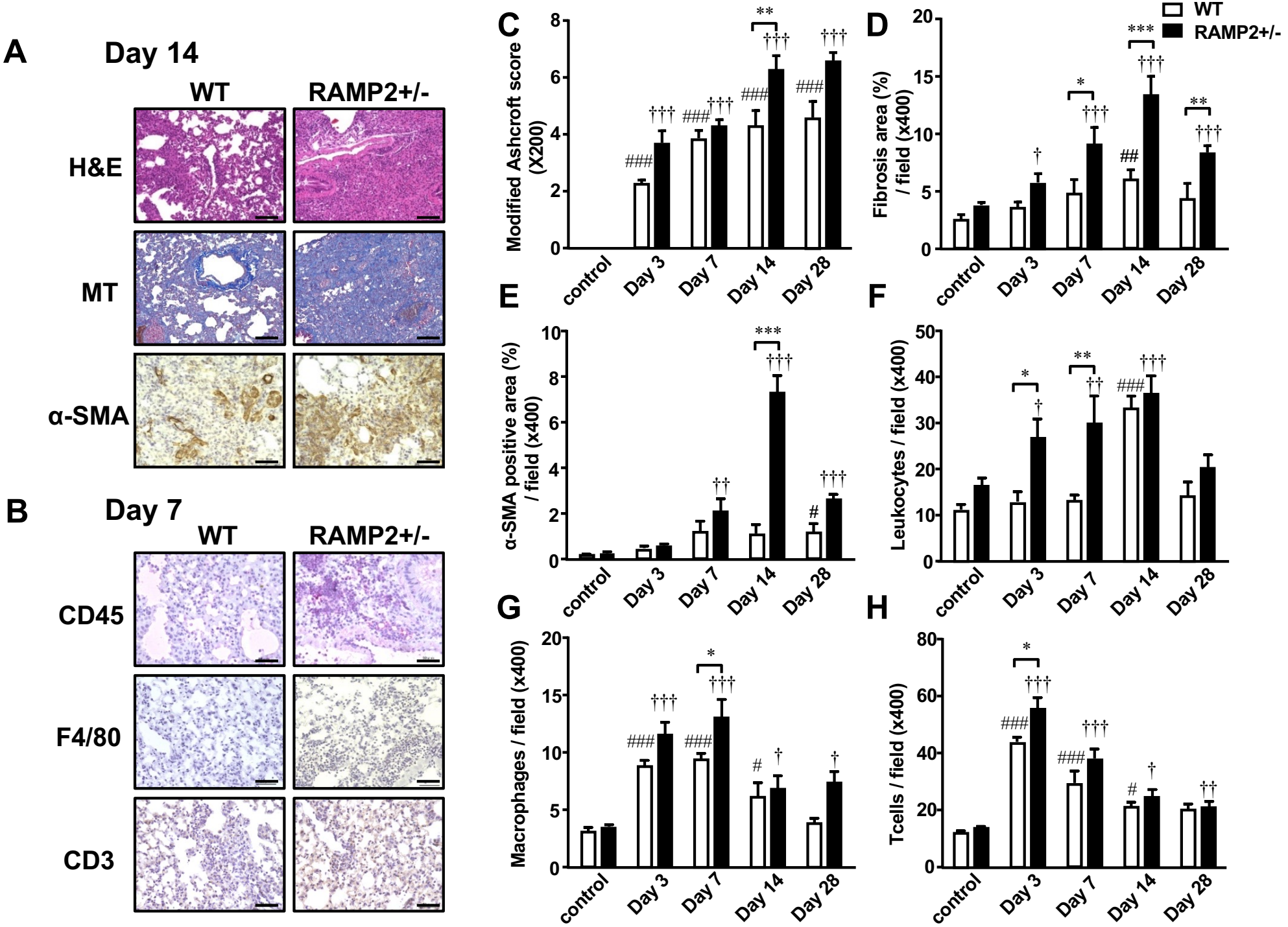

Supplementary Figure 6

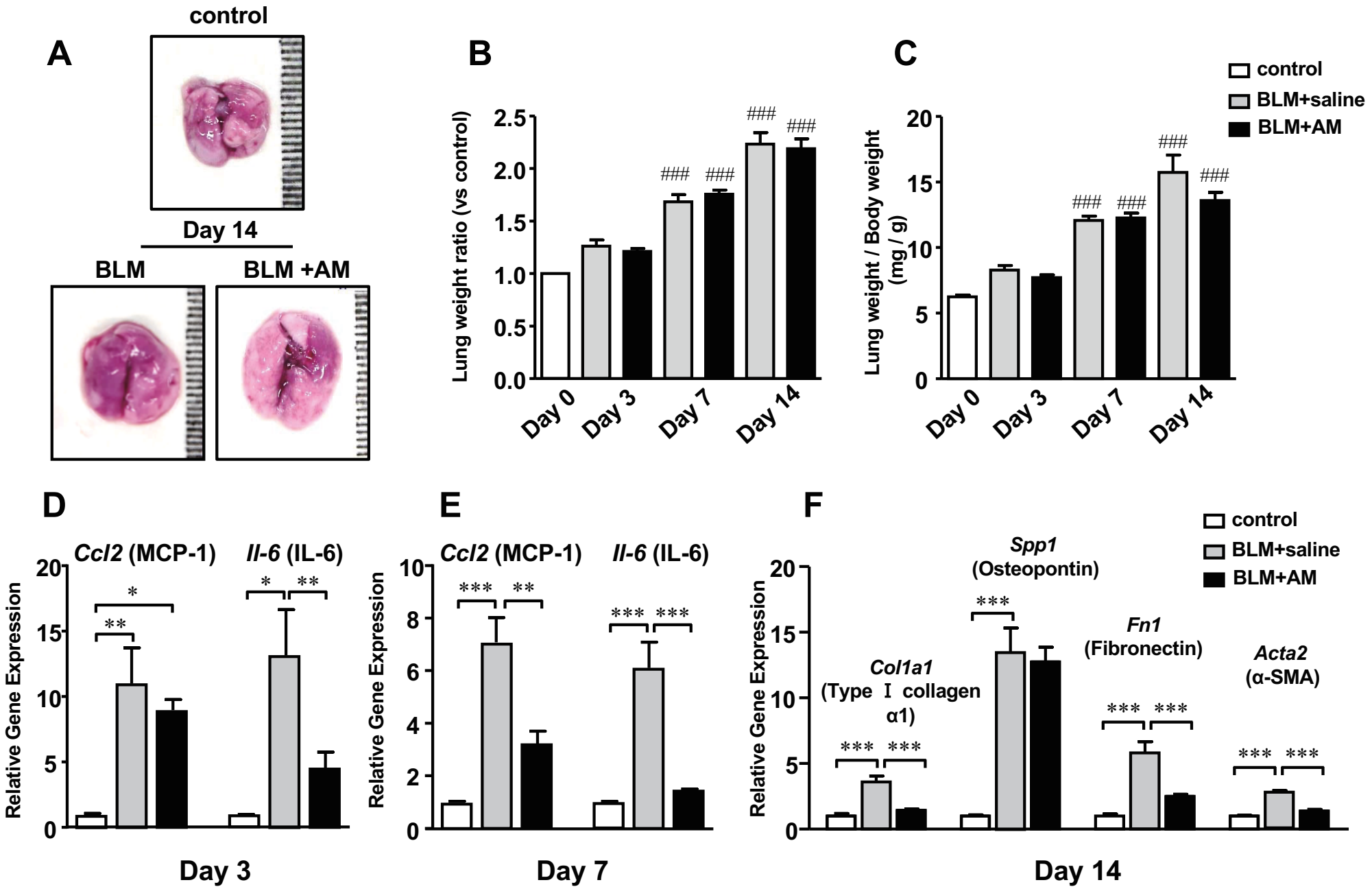

Supplementary Figure 7

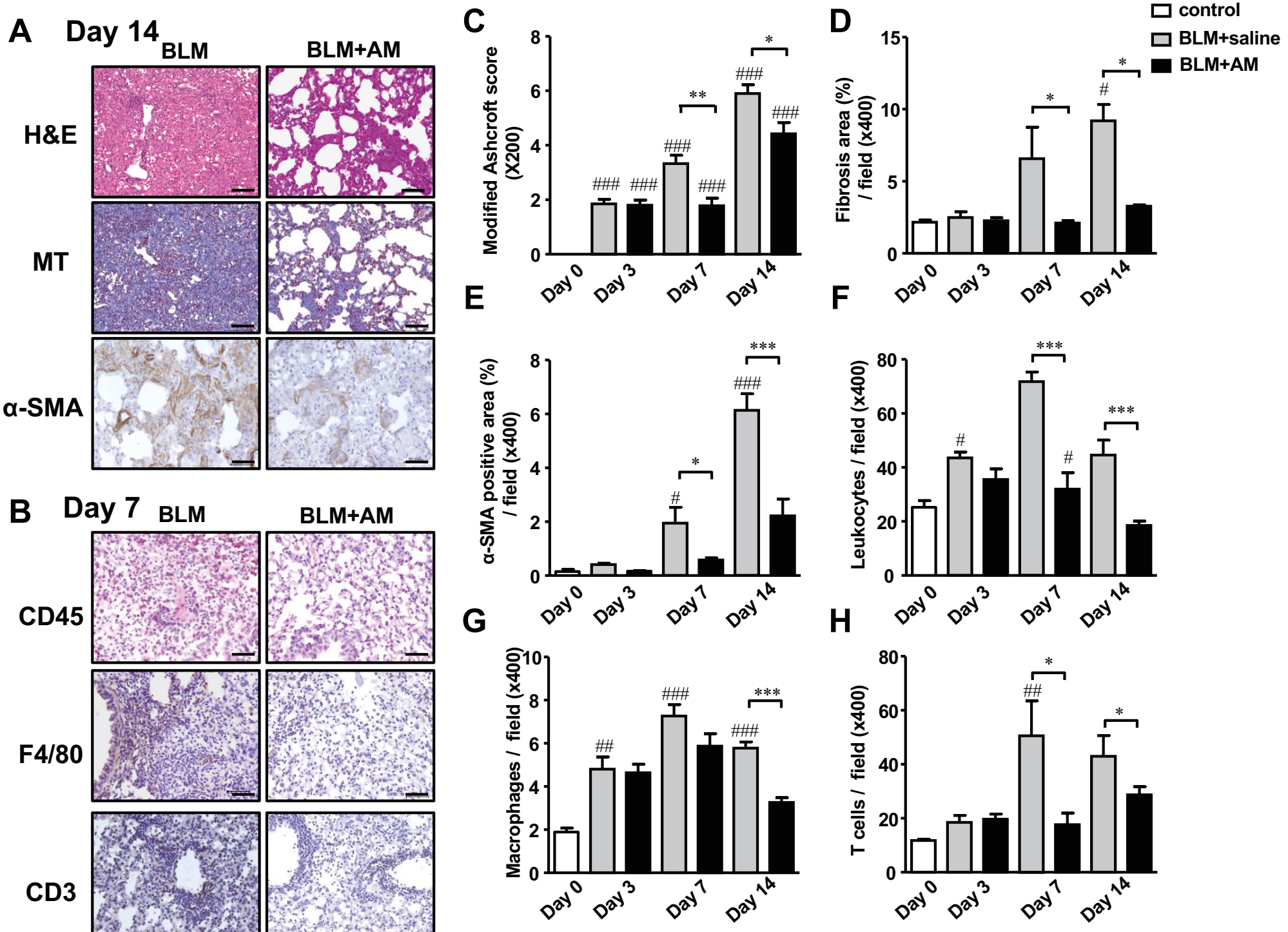

Supplementary Figure 8

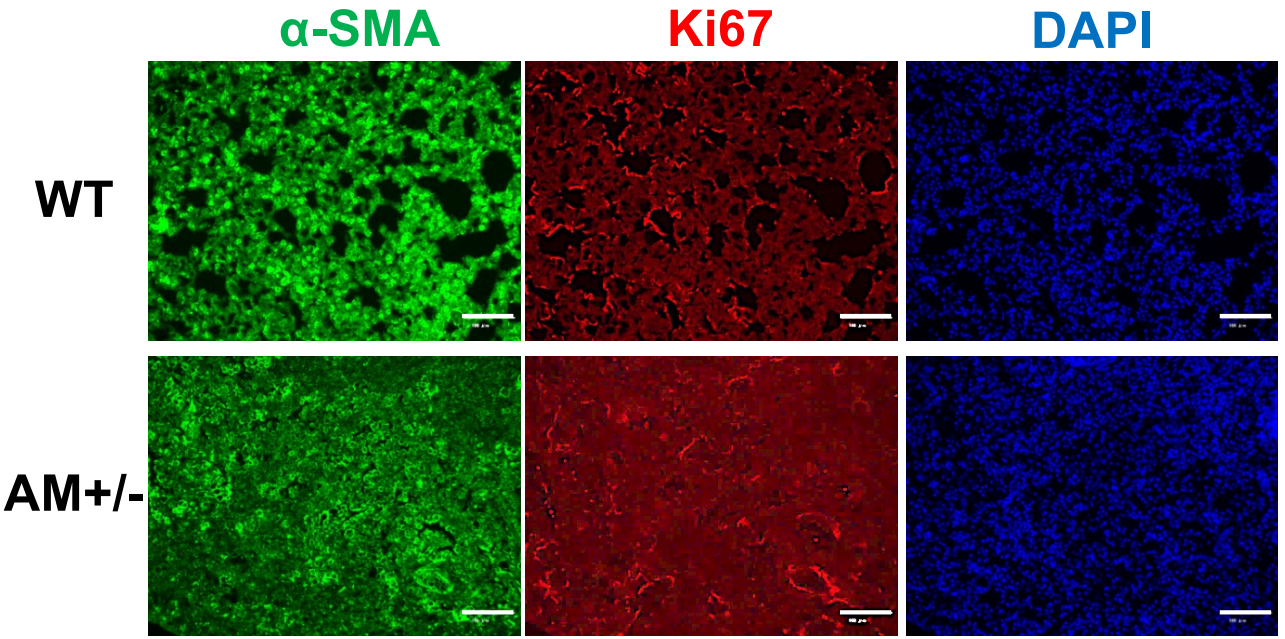

Supplementary Figure 9

Click here to download Supplemental Repository Link – FOR REVIEW ONLY

http://datadryad.org/stash/share/BcTuisq6yPVsvRbjB5LVnaFGxt2rixjusn